ELSEVIER

Surface Science 491 (2001) 303–332

SURFACE SCIENCE

www.elsevier.com/locate/susc

Atomic force microscopy of biomaterials surfaces and interfaces

Klaus D. Jandt *

Department of Oral and Dental Science, Biomedical Engineering and Biomaterials Science Section, University of Bristol, Lower Maudlin Street, Bristol, BS1 2LY, UK

Received 7 November 2000; accepted for publication 29 May 2001

Abstract

The use of atomic force microscopy (AFM) in biomaterials science and engineering applications has increased rapidly over the last few years. Beyond being merely a tool for measuring surface topography, AFM has made significant contributions to various biomaterials research areas dealing with the structure, properties, dynamics and manipulation of biomaterials surfaces and interfaces. This paper critically reviews methodological approaches and presents aspects of this research. Selected examples presented include micro and nanostructure and properties of biomaterials surfaces, molecular level interactions at biomaterial–biomolecule interfaces, interfaces between biomaterials and mineralised tissues as well as advances of mineralised tissue research. In these areas, AFM is shown to be a useful and versatile tool to study micro and nanostructure, to probe mechanical properties or to investigate dynamic process at biomaterials surfaces and interfaces.

Keywords: Surface structure, morphology, roughness, and topography; Biological molecules – proteins; Titanium; Etching; Surface chemical reaction; Physical adsorption; Solid–liquid interfaces

1. Introduction

Scanning probe microscopy (SPM) and especially atomic force microscopy (AFM) [1] have changed modern natural sciences by contributing to major progress in the understanding of the structure and properties of condensed matter [2]. AFMs are nowadays part of the standard equipment in almost every research or development department dealing with the characterisation or engineering of materials surfaces and interfaces. Similarly AFM has found numerous applications in the biological sciences based on its ability to explore samples under a variety of environmental conditions [3–5]. For example imaging of biomolecules with molecular resolution under aqueous conditions was not possible until the introduction of the AFM and its fluid cell [6,7].

More than 25 different SPM techniques are currently known [8] and new SPM techniques continue to be developed. Nevertheless, the vast majority of publications referring to SPM use either the scanning tunneling microscope (STM) or the AFM as experimental techniques. STM, which measures a quantum mechanical tunneling current between a metallic tip and a conductive surface,

* Tel.: +44-117-928-4418; fax: +44-117-928-4780.
E-mail address: k.jandt@bris.ac.uk (K.D. Jandt).

0039-6028/01/$ - see front matter
PII: S0039-6028(01)01296-1

was dominant in the research in early stages of the history of SPM since it was the first scanning probe microscope to be developed. Today AFM and its subtypes are by far the most dominant techniques in publications reporting research using SPM.

The main application of AFM is high resolution imaging of different material surfaces including metals [9], polymers [10], ceramics [11], biomolecules [12] or cells [13]. When ultra-flat and rigid surfaces are used, AFM allows true atomic resolution to be obtained [14]. The use of the AFM fluid cell allows one to observe and study processes such as protein folding [15] under aqueous conditions and in real time. A number of different AFM operation modes allow different structural and property details of samples to be probed. AFM and its subtypes measure sample properties such as surface topography [1], frictional sample properties with frictional/lateral force microscopy (FFM/LFM) [16], lateral chemical surface composition with chemical force microscopy (CFM) [17], differences in elasticity with force modulation microscopy (FMM) [18] and magnetic properties with the magnetic force microscope [19]. This list of different AFM subtypes covers only some of the most prominent microscopes and working modes developed so far.

The unique resolution of most AFM techniques is based on the ultra-sharp AFM probes (tips with radii of typically 4–60 nm) attached to a flexible cantilever and accurate ceramic piezoelements which allow the sample to be scanned in the x–y plane with sub-nanometre precision. The piezoelements move in z-direction, for example to maintain a constant force between the probe and the sample. The AFM tip scans over the sample surface and the AFM records interactions between the tip and the surface. Tip sample interactions include electrostatic repulsion and van der Waals attraction as described by the Lennard-Jones potential, capillary forces and frictional forces.

The characteristic AFM features allow pN forces between individual molecules and surfaces by single molecule force spectroscopy (SMFS) to be measured. The nanomechanical and nanoconformational characteristics of the molecule can be studied by measuring the force–distance curves of molecules attached with their one end to the AFM tip and with their other end to the surface of interest. Often, more than one molecule is attached to the AFM tip in these experiments. Examples of molecular force spectroscopy include studies of the conformation of proteins [20], polymers [21], DNA [22] and receptor–ligand interactions [23].

In addition, the sharp AFM probe and the precise piezoelements allow matter on a nm scale to be manipulated. This area of SPM application is called nanomanipulation or nanoengineering. Examples of this are using the AFM tip to operate single wall carbon nanotubes as molecular switches with controllable reversibility [24] or moving individual gold nanoparticles on a Si/SiO_2 surface with an AFM tip in liquid [25].

It is obvious that SPM is a flourishing technology throughout the physical, materials and biological sciences. Nevertheless, despite its intensive use in other sciences, SPM techniques are currently only used sparsely in biomaterials science. A simple literature enquiry with the keywords 'biomaterial', 'AFM' and 'force microscopy' in June 2000 [1] delivered 88 articles whereas using only the last two keywords finds 5325 articles. At the Sixth World Biomaterials Congress in May 2000 [26] approximately only 1% of the presented papers used AFM as a research method. Nevertheless, biomaterials research using AFM techniques is very exciting and at the cutting edge of the field.

AFM methods match important needs in biomaterials science. Biomaterials can be defined as non-viable materials used in (medical) devices, intended to interact with biological systems [27]. Biomaterials scientists and engineers face the challenge of exploring structure-property relationships of biomaterials on ever-smaller scales. This need arises from the decreasing structure sizes of functional units in biomaterials systems such as cardiovascular implants, dental materials, drug delivery systems, engineered tissues or the under-

[1] Institute for Scientific Information (ISI), Bath Information and Data Services (BIDS), http://www.bids.ac.uk/ (24 June 2000) including all journals of the science citation index (SCI). Wildcards for the endings of the search terms (e.g. force mircoscop*) have been used to maximise the number of articles found. The period of the literature was 1996–2000.

standing of the principles of biocompatibility. The biomaterials scientist is especially interested in the structure, surface roughness, chemistry, and mechanical properties of biomaterials, and in studying the interaction of biomaterials with biological matter. Some of these properties and interactions can be studied with traditional microscopy techniques, such as electron microscopy (SEM, TEM) and these studies are sometimes complemented by spectroscopic methods. Electron microscopy methods, however, often require sophisticated sample preparation methods, such as etching techniques or metal evaporation onto the samples, which can lead to artefacts and the loss or change of detectable information of the sample structure and properties. AFM measurements often do not require additional sample preparation, hence leaving the material and its properties in its native state.

This paper reviews research relevant for biomaterials science and engineering which uses AFM as a tool. Rather than trying to cover all research carried out in this area, this paper presents selected examples and demonstrates how useful AFM is for the biomaterials scientist and biomedical engineer.

2. Instruments, operation modes and methods

2.1. AFM principle

The main SPM type currently used in biomaterials science and engineering applications is the AFM. This section therefore focuses on the AFM principle and its operation modes. In addition, important AFM subtypes are discussed in this paper briefly. Details about SPM methods, instruments and instrumental evolution not covered in this paper can be found elsewhere [2,28–30].

As opposed to optical or electron microscopes, scanning probe microscopes such as the AFM do not use glass or magnetic lenses for producing an image of the sample but a sharp tip (probe). The resolution of an AFM depends strongly on the shape of the tip [28]. The smaller, i.e., sharper the tip is, the smaller is the surface area sampled by this tip. An AFM tip consists of a microfabricated pyramidal Si or Si_3N_4 tip (typical radii: 10 nm for etched Si tips and 20–60 nm for standard Si_3N_4 tips, respectively) attached to a flexible cantilever of a specific spring constant. The cantilever deflects in z-direction due to the surface topography during tip scanning over the sample surface. Fig. 1 shows the principle set-up of an AFM. A four segment photodiode detects the deflection of the cantilever through a laser beam focused on and reflected from the rear of the cantilever. A computer processes the electrical differential signal of the photodiode obtained from each point of the surface and generates a feedback signal for the piezoscanner to maintain a constant force on the tip. This information is transferred into a topographic image of the surface. The main forces contributing to the cantilever deflection are electrostatic (Coulomb) repulsive forces and attractive van der Waals forces between the atoms within the tip and the atoms of the sample surface. Hence, the AFM is also called scanning force microscope. In practice, however, other forces such as capillary or electrostatic forces may also contribute to the image data obtained [31], which sometimes may complicate the interpretation of the AFM data obtained.

At the beginning of the imaging process the AFM tip is brought either into direct contact with the sample surface, or is kept very close above ($d \approx 0.1$–10 nm) the surface of the material to be investigated. Physical contact or a small distance between the tip and the material surface allows specific physical interactions such as van der Waals forces to take place. Since interactions between the tip and the sample surface such as van der Waals interactions decrease rapidly with the distance between the tip and the sample surface the AFM's resolution of 0.2 nm lateral and 0.001 nm vertical is unsurpassed by any other non-SPM method.

Assuming bond energies for ionic bonded samples of $U \leqslant 10$ eV and 10 meV for van der Waals bonded samples (such as organic crystals) and taking the repulsive force as acting through a distance $\Delta x \approx 0.02$ nm the interatomic force

$$F = \frac{-\Delta U}{\Delta x} \tag{1}$$

would be $\leqslant 10^{-7}$ N for ionic bonds and $\leqslant 10^{-11}$ N for van der Waals bonds [32]. These values define

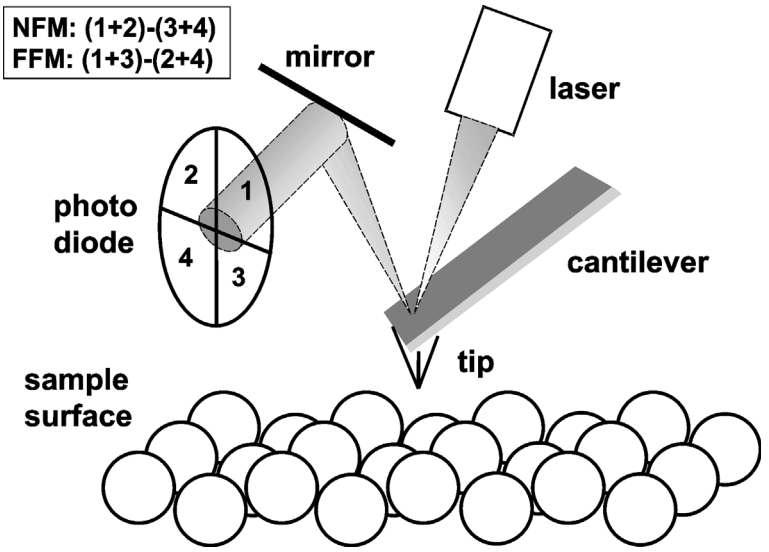

Fig. 1. Schematic representation of an AFM. The cantilever-tip system is deflected by the surface topography of the sample. Cantilever deflections are detected with a laser-optical set-up. The four-segment photodiode detects normal forces (normal force microscopy (NFM)) and frictional forces (FFM) affecting the tip. In most AFM systems the sample rests on a piezotube scanner (not shown in this figure) which allows a scanning motion in x- and y-direction as well as movement in z-direction.

the requirements for the force applied by an AFM probe, i.e., the force constant of the cantilever. Microfabricated Si_3N_4 flexible cantilevers [33] used on soft biomaterials have typical force constants of 0.0006–2 Nm^{-1} which help to minimise the forces applied to the sample by the AFM. Typical resonance frequencies of the cantilevers are 3–120 kHz. Typical slopes of pyramidal Si_3N_4 or Si tips are 55° with smooth side walls [33] and with tip radii ranging from 20 to 400 nm allowing the tip to slide with low friction over rough surfaces. Different AFM operation modes (see Section 2.2) may require using different kinds of AFM tips. A number of different cantilever-tip systems with a wide range of spring constants and tip radii and shapes are available, which allows the appropriate tip for a sample to be chosen.

The second specific component of an AFM is a piezoelectric scanner, often tube shaped [34]. This scanner coverts electric signals supplied from the AFM control electronics into mechanical scanning motion in the lateral direction of the sample. SPM piezoscanners are produced from zirconate titanate ceramics (PZT). PZT is the trade name of the lead zirconate titanate piezoelectric ceramics by one major producer, Vernitron. It is also commonly used in the scientific literature as a standard acronym. During production, a poling process induces a strong piezoelectric effect in this material [35]. Piezo scanners should be calibrated every few months to allow reliable spatial measurements with the AFM. To that end, high-resolution AFM measurements of atomic flat test samples with well-known lattice constants are performed. Typical samples for this procedure are highly oriented pyrolitic graphite (HOPG) or mica. The measured atomic distances of the sample are then compared with the known values obtained with other methods and the calibration of the scanner is adjusted if necessary. Long-tube scanners respond non-linear to low voltages [28]. The software of the AFM control computer corrects for this non-linearity. For other, lower resolving SPM techniques the scanner calibration can be done in a similar way to that described above by using calibration samples such as gratings for which the dimensions are known from other techniques (e.g. high resolution scanning electron microscopy).

During the scanning process the tip detects local changes of the physical property of interest,

leading to an image of the measured physical property of the sample. In some systems the probe is attached to the piezoscanner whereas in other systems the sample is attached to the piezo unit, enabling a relative motion of probe and sample in both cases. The piezos are constructed as tubes consisting of a number of segments which enables a two-dimensional scanning motion in an x–y plane as well as a motion in z-direction to vary the distance between the probe and the sample. The latter is needed for maintaining chosen distances and forces between the tip and the sample surface. A feedback mechanism in the AFM controller accomplishes this. The electronic part of the AFM consists of a computer and a controller unit which are used for signal acquisition and processing and which supply the electric signals required to drive the AFM.

2.2. AFM operating and imaging modes

The AFM can operate in different modes. In the constant force mode (Fig. 2a) the force (which is proportional to the cantilever deflection in z-direction) between the tip and the sample surface is kept constant via an electronic feedback loop. In this mode the tip is in permanent physical contact with the sample. This AFM operation mode is called contact mode. An image of the sample's surface topography is created from the cantilever deflection required to maintain a constant force over the surface. Monitoring the signals received from the photodiodes and keeping this signal at a given level via a feedback loop accomplishes the latter. The feedback system feeds its signal into the z-component of the piezoscanner, which maintains the force to the cantilever at the given level through appropriate movement in z-direction.

Contact mode can be used to image hard and stable samples which are not affected by the frictional force components the tip applies to the sample. Therefore, the constant force mode may not always be appropriate for biomaterials applications especially when weakly adsorbed biomolecules are observed. Typical forces applied in constant force mode are in the order of nN but can be varied over a wide range as cantilevers with different spring constants are available.

In constant force mode measurements additional to the surface topography can be performed. Since the tip is in permanent contact with the surface, the scanning motion of the system leads to some torsion of the cantilever in the lateral x–y plane. This torsion reflects the frictional properties of a surface and can be monitored by the photodiodes. Measurements of this kind are called LFM [16] or FFM. If the tip is modified with functional groups, such as $-CH_3$ (hydrophobic) or –COOH (hydrophilic) and the microscope operates in the LFM mode, hydrophobic or hydrophilic areas on the sample surface can be detected with nm resolution. Similar chemical groups at the tip and the sample surface interact more than dissimilar groups. A stronger interaction leads therefore to a higher friction between the tip and the sample. This kind of experiment, which requires some experience in tip preparation, is therefore called CFM [17]. Nevertheless, it is not always necessary to chemically modify AFM tips to obtain a chemical sample contrast. It has been shown that the lateral chemical composition of block copolymer samples can be obtained with native (unmodified) AFM tips in the FFM mode [36] with nm resolution. CFM and FFM appear to be particularly attractive for the investigation of active biomaterials with functionalized surfaces such as drug delivery devices or laterally patterned surfaces.

Lateral tip–sample interactions such as frictional effects are not always welcome when performing AFM experiments, especially when very soft surfaces are to be imaged. To reduce frictional interactions and damage of soft samples, other imaging modes have been developed. These modes, which use an oscillating cantilever in z-direction, are called dynamic imaging modes. Three main dynamic modes are most common: tapping mode, the so-called phase imaging and the force modulation mode.

Tapping mode (Fig. 2b) [37] uses an oscillating tip (frequencies in air 50–500 kHz, in fluids approximately 10 kHz) at a tip amplitude of several tens of nm if the tip is not in contact with the surface. If the oscillating tip, which is driven by an oscillation piezo, moves towards the surface, it begins to touch or 'tap' the surface. This surface

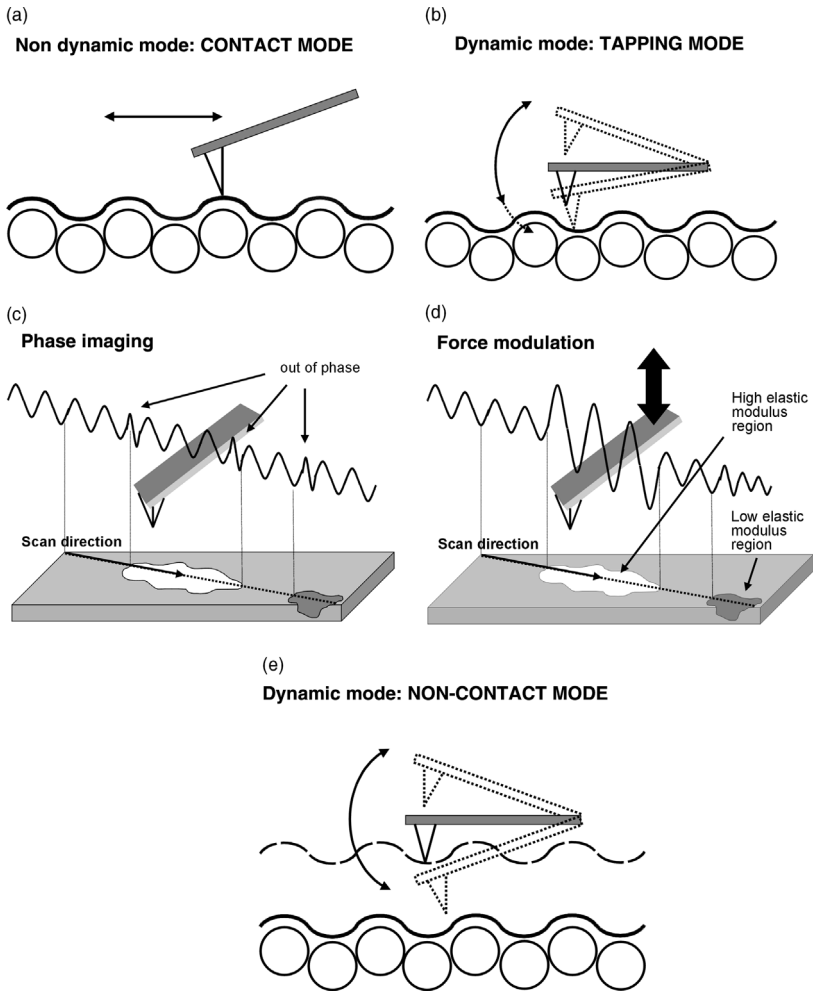

Fig. 2. (a)–(e): Four common AFM operation modes. In contact mode (a) the tip is in permanent contact with the sample surface. Owing to the permanent tip–sample contact the shear forces applied to the sample during scanning are significant and potentially damaging to weakly bound molecules such as proteins adsorbed on biomaterials. Nevertheless, contact mode enables extreme high resolution and allows recording FFM images with the AFM. (b) Shows the AFM tapping mode, which uses a tip oscillating at typically 25 kHz. Since the tip is not in contact with the sample during lateral movement during scanning, shear forces applied to the sample by the tip are negligible. Similar to the contact mode, the tapping mode provides information about the sample topography. In AFM phase imaging shown in (c) variations in materials viscoelasticity lead to different phase lags of the cantilever oscillation, relative to the signal sent to the cantilever's piezooscillation driver. This phase lag is simultaneously monitored by the AFM control electronics, recorded and transformed into AFM images. AFM phase imaging gives non-quantitative information about hardness and elasticity of samples. (d) shows the force modulation mode (FMM). Compared to tapping mode, in this mode an additional sinusoidal modulation is applied to the cantilever while the tip scans the surface. Thus, the contact force applied to the sample is modulated. From the RMS amplitude of deflection of the cantilever, information about the mechanical properties (stiffness) of the sample can be obtained with a lateral resolution of about 10 nm or better. For a given amplitude modulation, the resulting RMS cantilever deflection for a soft material will be less than for a hard material. Thus, the measured RMS amplitude at each point of the sample surface is used to measure local differences in the elasticity of the sample. In non-contact AFM modes shown in (e), the cantilever tip is placed at the attractive force region (i.e., attractive van der Waals forces), and force gradients are detected. The attractive forces are usually small compared to repulsive forces. The force gradients can be detected either from shifts in the resonance frequency of the cantilever or the amplitude and the phase of the cantilever. The advantages of these approaches are the high sensitivity of gradient measurements and that small forces are applied to the sample.

contact leads to an energy loss of the oscillating tip, which reduces the tip amplitude significantly. The reduction of the oscillation amplitude is used to identify and measure surface topographic features. The average cantilever deflections are used as an input signal into the feedback loop similar to conventional contact mode AFM to maintain a constant average applied force. Tapping mode operates also in fluid environments. Therefore, the AFM mode is most often used in biomaterials science, due to the relatively small interactions between the tip and the sample, especially in the lateral direction of the surface.

Phase imaging (Fig. 2c) [38] can be performed at the same time as topographic imaging with tapping mode in a single scan. The phase imaging mode takes advantage of the fact that the tip–sample interactions do not only depend on the sample's topography but also on different sample characteristics for example sample hardness and elasticity or adhesion. In tapping mode the cantilever's oscillation amplitude is used as a feedback signal to measure topographic variations of the sample. Variations in materials properties mentioned above lead to a phase lag of the cantilever oscillation, relative to the signal sent to the cantilever's piezooscillation driver. This phase lag is simultaneously monitored by the AFM control electronics, recorded and transformed into AFM images. AFM phase imaging gives non-quantitative information about hardness and elasticity of samples. For example, a flat polymer sample containing two different polymers with different stiffnesses at the surface may be distinguishable in the AFM phase mode although the two polymers would not be distinguishable from the AFM surface topography image [39]. Phase imaging can also act as a real-time contrast enhancement technique because phase imaging highlights edges. Fine features, such as surface steps or edges, which can be obscured by a rough topography are revealed more clearly through phase imaging.

Closely related to the tapping mode is the force modulation mode (Fig. 2d) used in FMM [18]. In this mode, however, an additional sinusoidal modulation is applied to the cantilever while the tip scans the surface. Thus, the contact force applied to the sample is modulated. From the root-mean-square (RMS) amplitude of deflection of the cantilever, information about the mechanical properties (stiffness) of the sample can be obtained with a lateral resolution of about 10 nm or better. For a given amplitude modulation, the resulting RMS cantilever deflection for a soft material will be less than for a hard material. Thus, the measured RMS amplitude at each point of the sample surface is used to measure local differences in the elasticity of the sample. FMM does not give absolute values of sample stiffness. Rather, different stiffnesses of the sample surface appear as areas of different image brightness in the FMM image.

The amount of force applied by the AFM tip to the sample can be even more reduced if non-contact [40] AFM modes are used for operation (Fig. 2e). In non-contact modes, the cantilever tip is placed at the attractive force region (i.e., attractive van der Waals forces), and force gradients are detected [40]. This is done since the attractive forces are usually small (below 1 pN [41] at tip–sample distances larger than 0.6 nm) compared to repulsive forces. The force gradients can be detected either from shifts in the resonance frequency of the cantilever [40] or the amplitude and the phase of the cantilever [42]. The advantages of these approaches are the high sensitivity of gradient measurements and that small forces are applied to the sample which make non-contact modes suitable for AFM imaging of soft biomaterial–biomolecule interfaces. High sensitivity is even given when the lever is comparatively stiff, and therefore is not subject to instability. Force gradients of 10 $\mu N\,m^{-1}$ or lower can be detected [43]. This gradient corresponds to a force as small as 0.1 pN at a probe gap of 1 nm, depending on the character of the force curve. The amplitudes of the lever oscillations are usually about 1 nm allowing detecting force gradients at a range of distances from the probe. Since long-range forces are involved at larger distances, the resolution of non-contact methods decreases with increasing probe distance from the surface. Phase-lock technology has been proposed [44] to stabilise the cantilever resonance when the lever is brought in very close proximity to the surface. Conventional systems tend to destabilise under these conditions. Although the operation range of the cantilever amplitude of the non-contact mode is

much smaller than for the tapping mode, and non-contact AFM is more complicated than the tapping mode, the real non-contact mode offers the lowest possible interaction between sample and tip which is an advantage for work on many soft biomaterials systems. It is expected that non-contact modes will be easier to use in the future and will be further improved. Recent research results [45,46] raise hopes that non-contact AFM may achieve true atomic resolution under a number of environmental conditions.

Commercial AFMs produce a number of different data types [47]. Height data show the surface topography of samples and correspond to the change in piezoheight needed to keep the cantilever deflection constant. In contact mode the differential signal from the top and bottom photodiode segments (see Fig. 1) generates deflection data. Deflection data collected with high feedback gains is essentially the derivative of the height data. This is often referred to as the error-signal mode and provides a sensitive edge detection technique. Height and deflection data can be collected simultaneously. In tapping mode the error signal is given by the amplitude data rather than the deflection data. Amplitude data describes the change in the cantilever amplitude and is edge sensitive. The generation of phase data has been described above. Fig. 3 describes the AFM imaging modes discussed.

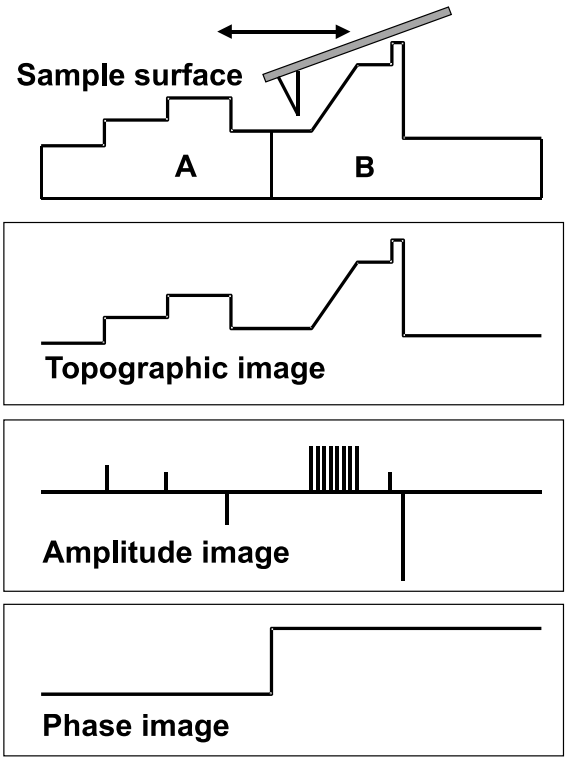

Fig. 3. Sketch demonstrating AFM imaging modes. The AFM tip scans a sample in tapping mode. The sample consists of two regions with different stiffnesses A and B. The topographic image gives information about the three-dimensional sample profile whereas the amplitude image is edge sensitive. The different stiffnesses of the regions A and B are reflected by the two different phase signals observed.

During AFM operation, image artefacts may occur. Experience of the operator, careful sample preparation and a thorough understanding of the AFM operation modes and tip–sample interactions are prerequisites to identify artefacts. Dull or multiple tips cause common artefacts. Blurred or ghost (double) images are the results of imaging with low quality tips. If an image artefact is suspected one should rotate the scan direction and change the magnification and the tip. If the observed structure is unaffected by any of the applied changes it is most likely not an artefact. More strategies to avoid artefacts can be found elsewhere [2].

2.3. Force–distance measurements with AFM

In addition to imaging of the surface topography and exploring the chemical and non-quantitative mechanical properties of samples, the AFM can be used for the measurement of force–distance curves. These curves provide quantitative information of forces between the tip and the sample as a function of tip–sample distance. Fig. 4 shows an example of a force–distance curve.

If the AFM tip is approached to the sample surface, the cantilever is deflected from its original position. For distances typically larger than 10 nm electrostatic and hydrophobic interactions are dominant between the tip and the sample. If the force between the tip and the sample is attractive, the cantilever bends towards the sample. At tip–sample distances below 10 nm the bending is mainly caused by the attractive van der Waals forces in the non-touching regime. If the tip is approached

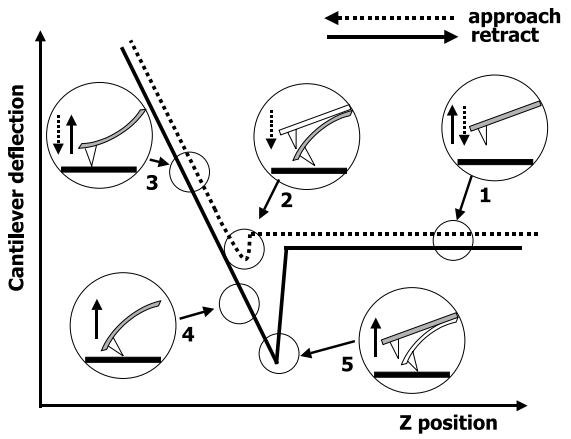

Fig. 4. Example of a force–distance curve. During the approach phase of the tip to the surface (1) there is no tip–sample contact. Tip–sample contact occurs at the point 2 where the tip jumps into contact to the sample due to van der Waals and electrostatic forces. The cantilever deflects further under an increasing force at the linear part the force–distance curve (3). When the movement of the piezoscanner retracts in z-direction the force of the cantilever is decreasing (3). Adhesive forces between the tip and the sample keep the tip in contact with the sample beyond the previous first contact force. This leads to a negative deflection of the cantilever (4). The cantilever then breaks free (5) form the surface (pull-out) and returns to its starting deflection (1).

further to the sample surface the cantilever jumps at a certain distance to the surface so that a rapid tip–sample contact is established (jump-in contact/touching regime). This happens if the attractive forces become larger than the spring constant of the cantilever. A further approach of the tip to the sample leads to a greater deflection of the cantilever. Depending on the forces applied, elastic or plastic deformation may occur to the tip, cantilever and/or the sample (indentation).

If the tip is subsequently retracted the bending of the cantilever is reversed beyond the distance of the initial jump in contact. The tip 'sticks' to the sample surface due to adhesive and capillary forces until an abrupt transition from the contact to the non-contact regime called pull-out occurs (see Fig. 4).

Capillary forces are important factors in force measurements taken in ambient air, but not in aqueous environments or in high vacuum. Since capillary forces may be larger than the intermolecular forces one is interested in, care has to be taken in the interpretation of force measurements obtained in an ambient air environment. More controlled experimental conditions such as force measurements in fluid solve this problem.

A prerequisite for obtaining exact force–distance relationships is the use of calibrated cantilevers of a known force constant. The force applied to the cantilever is given by

$$F = kz \tag{2}$$

where k is the spring constant of the cantilever and z is the deflection of the cantilever in z-direction perpendicular to the sample surface. Forces applied with an AFM tip to a sample surface can be estimated from the force–distance curves and the spring constant of the cantilever given by the manufacturer. Due to production tolerances, however, the spring constants may vary and significant differences between the actual and the specified spring constants are common [48]. Therefore, exact spring constants need to be determined for precise force measurements.

Different methods of determining the spring constants of cantilevers with high accuracy exist [49–51]. One method [49] relies on attachment of masses to the cantilever and measuring the resonance frequency shift between the unloaded and the loaded cantilevers whereas other methods require the determination of the unloaded resonant frequency of the cantilever, a knowledge of its density or mass, and its dimensions [50]. A simple and elegant method for measuring the force constant, resonant frequency, and quality factor of an AFM cantilever spring and the effective radius of curvature of an AFM tip has been presented by Hutter et al. and uses a thermal vibration approach to calibrate the cantilever [51].

Force–distance data collection can be either done at few points of the sample surface or, if the AFM is equipped with the necessary data acquisition accessories, at each point of the sample surface [40,52,53]. In the latter case, it is possible to obtain the force–distance curves, for each image point the AFM records. The measurement of an array of force–distance curves is called force volume. Force volume measurements take significantly more time to record than normal AFM

images. Therefore, this method appears to be unsuitable to record rapidly occurring surface processes. Force volume AFM operation can also be used to investigate the elastic properties of a material by measuring the force required to indent or deform each point of the sample surface. Force volumes can therefore, be used to produce microelasticity maps of the sample that show local variations in surface stiffness [54].

Force–distance curves can be measured either of direct tip–sample surface interactions or between a tip on which a molecule has been grafted and a surface. Using AFM tips functionalized with biomolecules such as proteins or antibodies can be considered to be AFM with (bio-) chemical sensitivity and molecular recognition abilities [55] since specific chemical interactions take place between the tip and the surface or molecule to be investigated. Examples include measurements of the debonding (rupturing) forces between receptors and ligands [23] or antibodies and antigens [56]. If a calibrated cantilever and calibrated piezoelements are used the debonding force between molecules attached to the tip and molecules attached to a surface can be measured and quantified SMFS.

Limits of force–distance measurements and molecular spectroscopy lie in the accuracy of the cantilever calibration and the piezocalibration. In the latter case hysteresis effects and creep may influence the measured force–distance curves and may falsify results. It is also under discussion if in the case of SMFS really only one molecule is attached to the AFM tip or if the measured force curves represent the interaction between the tip and more than one molecule attached to a sample surface.

Questions remain as to how far quantitative mechanical measurements such as the elastic modulus or hardness with AFM force–distance curves can be carried out reliably. For these measurements a well defined and known tip geometry in addition to an accurate normal loading of the force to the sample is required, both of which are not the case in most AFM experiments. AFMs equipped with nanoindentation accessories, which use a vertical transducer system for the precise measurement of force displacement curves, appear to solve these problems and may lead to more reliable mechanical measurements.

2.4. AFM nanoindentation

Recently, nanoindentation and hardness testing with SPM has become available in laboratories [57–61] and commercially [62,63]. The indentation process and the imaging are performed with the same tip in subsequent steps. Tips used for this procedure are often made of diamond. Special software enables a single indent or distinct patterns in sample surfaces. Subsequently, the indentation mode is left, which automatically reactivates the imaging mode and allows immediate observation of the indentations at the surface. Due to the lack of knowledge of the AFM tip geometry and unwanted bending or twisting of the AFM cantilever the exact indentation area and indentation angles are difficult to control in most AFMs. Therefore, the calculation of hardness and elastic modulus obtained with AFM is not straightforward and AFM indentation experiments lead often to relative hardness values only.

More promising appear to be AFM nanoindentation systems using a vertical transducer and well shape-defined diamond tip (for example a Berkovich tip) (Fig. 5) [63]. This transducer is used in combination with a normal AFM where the cantilever and the laser-optical detection system are replaced by the transducer-tip system. The normal (perpendicular to the sample surface) force loading of the nanoindentation system avoids loading not parallel to the z-axis, which occurs with the normal AFM set-up. The vertical displacement is monitored via a capacitive transducer set-up (Fig. 6) with 0.2 nm resolution. Since during the indentation process all displacements occur within the transducer, calibration problems with the PZT piezoscanner of the AFM are eliminated.

During indentation the applied load P and the depth of penetration h into the sample are continuously monitored leading to highly reproducible force–displacement curves [64–66] such as shown in Fig. 7. These curves in combination with the indentation area allow calculation of sample hardness and the reduced elastic modulus

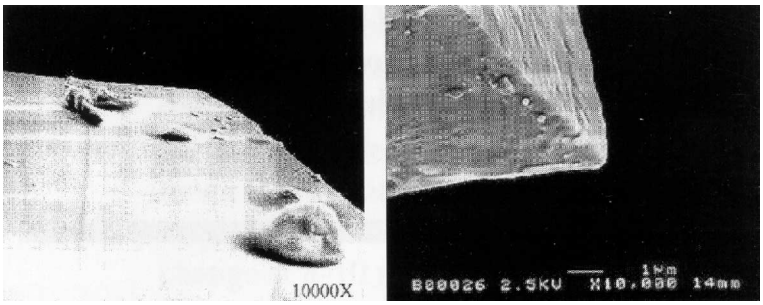

Fig. 5. Examples of indenter tips used for vertical transducer AFM nanoindentation. Left image: Berkovich tip (142°) with a nominal radius of 150 nm. Right image: 90° cube corner tip with a tip radius of 100 nm. These tips are much more blunt than normal tips (typical tip radius of tapping mode AFM tips ≈20 nm) used for AFM imaging. Images courtesy Dr. Thomas Wyrobek, Hysitron Inc. Minneapolis, NM, USA.

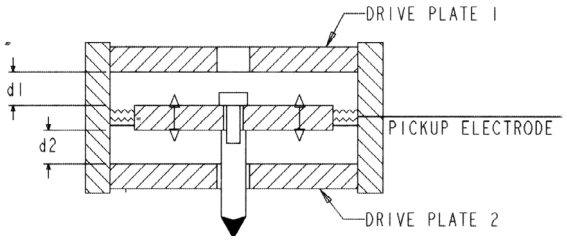

Fig. 6. Depiction of the vertical transducer used in AFM nanoindentation. A pickup electrode with an attached nanoindentation tip is suspended with fine springs between two capacitive driver plates. Small changes of the vertical z-position of the tip and therefore the pickup electrode lead to capacity changes of the system and are recorded by the nanoindentation electronics. Compared to the laser-optical set-up of a conventional AFM, this indenter tip set-up allows higher load-displacement control and normal (perpendicular) loading. For nanoindentation the applied loads are normally higher (>1 μN) than for normal AFM and the resolution in the x–y plane (a few nm) is not as good as with normal AFM. Image courtesy Dr. Thomas Wyrobek, Hysitron Inc. Minneapolis, NM, USA.

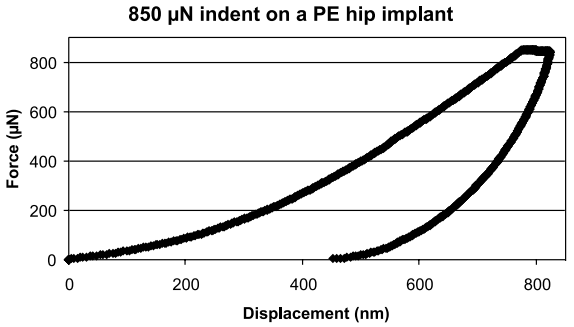

Fig. 7. Force–displacement curve of an indentation into a previously implanted HDPE hip implant with a vertical transducer nanoindentation AFM. The applied load was 850 μN. The left part of the curve was recorded during indentation whereas the right part of the curve was recorded during retraction of the tip from the identity. The hysteresis of the curve is caused by a plastic deformation of the material. Image courtesy Dr. Seth Downs and Dr. Thomas Wyrobek, Hysitron Inc. Minneapolis, NM, USA.

$$E_r = S\frac{\sqrt{\pi}}{2\sqrt{A}} \tag{3}$$

where S is the unloading stiffness dP/dh and A is the projected contact area [67]. The reduced modulus is related to the modulus of elasticity E through

$$\frac{1}{E_r} = \frac{(1-v_1^2)}{E_1} + \frac{(1-v_2^2)}{E_2} \tag{4}$$

where the subscript 1 corresponds to the indenter materials, the subscript 2 refers to the indented materials and v is Poisson's ratio. For a diamond indenter tip E_1 is 1140 GPa and v_1 is 0.07 [59]. The Poisson ratio varies between 0 and 0.5 for most materials. The hardness H is defined by the ratio of the maximum load P_{max} to the projected contact area A [67]:

$$H = \frac{P_{max}}{A} \tag{5}$$

For a Berkovich indenter the projected contact area is $A = 24.5\ h_c^2$ where h_c is the contact depth [67].

The defined tip geometry and the transducer technology allow good load/displacement control. The small size of the indentation tip allows the application of small loads in the order of nN to μN. Certain limitations of this method apply. Tip deformation may occur on hard surfaces, but does not occur for soft samples like cell membranes. One of the main difficulties is to determine the tip contact area on soft samples. The lateral imaging resolution is limited to about 10 nm due to the tip radius. Flat samples are required, there are limits to the indentation depth and some questions about the exact calibration of these systems remain.

2.5. Sample preparation for AFM

It should be emphasized that all methods mentioned here do not require any surface coatings of the samples, i.e., AFM techniques are direct imaging techniques with extreme resolution. AFM imaging is subject to artefacts caused by damage to fragile structures on the surface. In practice that means that soft materials, such as weakly adsorbed protein molecules, pellicle or smear layers on biomaterials or tissues can be challenging to image. Soft structures must be immobilized in order not to be swept away by the scanning tip and should be imaged in a fluid environment by using a so-called fluid cell which contains the tip, the sample and a clear fluid such as water or a buffer solution. As a result of imaging in fluid, capillary forces are reduced and soft samples can be imaged.

The fluid cell also allows the imaging of for example real-time processes such as the dissolution of mineralized tissues exposed to acids [68] or to image proteins in buffers [69], thus avoiding conformation changes due to drying. The ability to image materials and molecules under aqueous condition is a major advantage AFM has over other microscopy techniques. This capability is most attractive to the biomaterials scientist as it potentially enables imaging of biomaterial interfaces under near to physiological conditions.

Modern AFMs allow all sample sizes to be used. The typical AFM imaging area, however, is limited by the physical constrains of the scanner to 1×1 nm^2–250×250 μm^2. The z-range of AFM scanners is limited to about 8 μm, so rougher samples or curved samples cannot be imaged. Samples should therefore be flat and clean.

For high resolution imaging of molecules flat substrates are required as support. A protein molecule of a diameter of a few nm placed on a substrate of a roughness of a few nm would not be visible in an AFM height image as it would be 'hidden' by the surface topography. Therefore, AFM imaging of single molecules has been carried out on a number of different flat substrates such as glass [69,70], silicon [71], HOPG [72] and mica [73,74]. The latter two substrates are the smoothest of this selection and have a typical surface RMS roughness of approximately 0.1 nm over an 1 μm^2 AFM scan area. HOPG can be reused by removing its top layers with adhesive tape whereas mica cleaves easily in a number of samples. The low costs of mica (a few cents per sample) compared to HOPG (a few hundred dollars per sample) have made mica one of the most commonly used substrates for AFM investigations.

To control the surface topography and chemistry of substrates self-assembled monolayers (SAMs) [75–78] have been used as substrates for AFM imaging. SAMs can mimic surface chemical properties of biomaterials such as those of different polymers by using hydrophobic terminating groups (e.g. alkyl). Another motivation to use SAMs as substrates is their ability to immobilise adsorbed molecules, which is desirable for AFM studies. Thus, interactions between proteins and surfaces as a function of a well defined surface chemistry [79] can be explored. Molecular attachment to SAM surfaces is often accomplished via non-specific interactions such as hydrophobic attraction. The covalent attachment of molecules to SAM is an alternative, which increases the bond strength and stability of the attached molecules significantly [80,81].

SAMs are ad hoc engineered model surfaces, which require pure chemicals and clean conditions during production. They appear to be ideal for fundamental AFM research of adsorbed macromolecules.

A number of approaches are available to study clinically relevant biomaterials used in prosthetic devices with AFM. Many surfaces of biomaterials and mineralised tissues show roughness [82,83]

that are beyond the limits of the AFM. Thus, a common strategy is to produce AFM samples with a reduced roughness and maintaining the biomaterial's surface chemical composition as far as possible. In the interpretation of the results obtained with these 'flattened' samples it should be kept in mind that the biomaterials surface roughness is a known modifier of histo-compatibility [82]. Strategies of reducing the roughness of samples include polishing [68], fracturing [84], microtoming [36,85] and spin coating on flat substrates [86]. A novel approach of producing atomically flat surfaces of TiO_2 is the titanium stripped template (TST) method [87]. A titanium film is evapo- rated on an atomically flat mica surface. Subsequently a resin is deposited on top of the Ti layer and after resin curing the mica is removed, leaving a clean, ultra flat TiO_2 surface. The surface chemical composition of this sample is similar to that of clinically used biomaterials and provides the flatness necessary for molecular studies of adsorbed human plasma fibrinogen and other proteins relevant for blood coagulation [87]. A related template stripping method has been shown previously to work for gold samples [88,89] and may potentially work for other biomaterials.

3. Biomaterial surfaces explored with AFM – materials aspects

The characterisation of biomaterials is an essential first step for the understanding of their performance in the host. Of special interest is the characterisation of internal and external interfaces of biomaterials as these determine the biomaterial's mechanical performance and the interaction with the host, respectively. AFM as a surface sensitive technique is a suitable tool to explore these phase boundaries.

There are different ways in which AFM can help to characterise biomaterials surfaces and interfaces. In the bulk characterisation of biomaterials AFM is used in fractographic testing [90] of composite biomaterials [84]. Fractography gives access to the inside of a bulk biomaterial by fracturing it in the final stage of a tensile test. The mechanisms of fracture that occur in a specimen are qualitatively interpreted by microscopic examination [90]. Recently, interest in fractographic studies in the field of oral biomaterials has risen significantly due to the introduction of new materials and the increased demands on their mechanical performance. Fractographic investigations have focused on the principles and methodology of the determination of the sites of fracture initiation [91] and the fracture behaviour of different oral biomaterials, such as dental composites [92,93,84]. Of special interest for these biomaterials is the bond between the microscopic silicon dioxide filler particles and the surrounding polymer matrix of Bis-GMA, a dimethacrylate type resin. Due to the different chemical properties of fillers and resin, compatibilisers such as silanes are used at the filler resin interface. Fig. 8a and b show results from a fractographic AFM study of light polymerised microfilled dental composite [84]. Height and cantilever oscillation amplitude data obtained in tapping mode were recorded. The composite contains 40% (vol./vol.) silicon dioxide fillers with a grain size of 0.02–0.07 μm (manufacturer's data). In addition, it contains isopropylidenbis [2(3)-hydroxy-3(2)-(4-phenoxy) propylmethacrylate], 2,2(4),4-trimethylhexamethyllenbis (2-carbamoyloxyethyl)-dimethacrylate and 3,6-dioxaoctamethylendimethacrylate resins and (3-methacryloyloxpropyl) trimethoxysilane as bonding agent between the silicon oxide filler particles and the polymer matrix. The AFM fractographic study showed the filler particles and the surrounding polymer matrix at the sample fractured surfaces. The filler particles are embedded firmly in the polymer matrix and no indication of filler pullout was observed. The silane rich polymer–filler interface showed a distinct, even rim of a width of 10 nm, which originates from plastic deformation of the silane reinforced interface indicating stress concentration at the interface during fracture. This result supports proposed models for the structure of the silane interface [94,95] and complementary experimental data obtained previously [96]. In addition to the structure information, the AFM measurements enabled to measure the roughness R_a of the fractured surfaces and the so-called fractal dimension, which is a measure for the level of geometric complexity of the fractured surface.

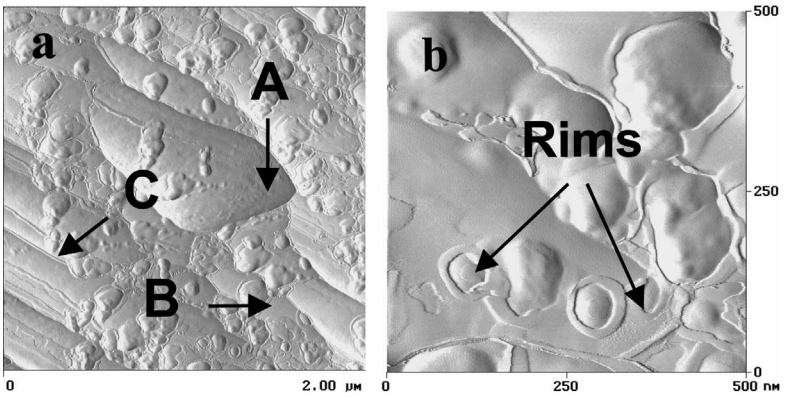

Fig. 8. (a) and (b): AFM amplitude images of fractured dental composite surfaces. Resin matrix (A) and filler particles (B) can be seen in (a). Fracture lines (C) separate different surface areas. The filler particles are firmly embedded in the resin matrix and no evidence of filler particle pullout was found. Distinct rims are surrounding most filler particles as can be seen in (b). These rims are likely to originate from the silane compatibilising agents used to bind filler particles to the resin. The width of the rims is a few 10 nm. Images after [84].

Both parameters are useful in the interpretation of fractured surfaces of biomaterials.

AFM is frequently used for the characterisation of polymeric biomaterials [97–102]. Surface morphology and order [97,98,101,102], composition and phase separation phenomena [99] or dynamic processes of polymer adsorption on HOPG [100] are typical examples for such studies.

Similar to the amplitude imaging of composite biomaterials (see above), AFM amplitude imaging supported by phase imaging has been used to identify surface microdomains in blends of the biodegradable polymers poly (sebacic anhydride) (PSA) and poly (DL-lactic acid) (PLA) [99]. The study showed the spherulitic structure of the semicrystalline PSA component and enrichment of the PLA at the PLA/PSA blend surface. The topographical data obtained in this study were unable to distinguish the two polymer components of the blend whereas the phase imaging revealed domains of the two components. In particular, it was shown that soft tapping on the sample surface generates a representation of topographical gradient changes across the sample surface in the phase image. When the tapping force was increased, these gradient changes were masked by the much larger phase changes induced by variations in surface mechanical properties.

Self-assembly of biomimetic surfaces of oligosaccharide surfactant polymers on mica has been studied in real time with AFM operating in tapping mode in fluid [100]. Oligosaccharide surfactant polymers mimic the protein non-adhesive properties of glycocalyx, the external region of cell membranes dominated by glycosylated molecules [100]. When HOPG is exposed to an aqueous solution of the surfactant polymer poly (*N*-vinyl dextran aldonamide-co-*N*-vinyl alkanamide) in an AFM fluid cell, it adsorbs on the graphite in ordered strands. The strands are aligned perpendicular to the substrate atoms. The adsorption process, which is driven by hydrophobic interactions and epitaxial adsorption of hexanoyl side chains onto the graphite lattice, was followed with the AFM for 20 h until a monolayer had formed. In this study the AFM's capability of following processes in real time and in a fluid environment, and to contribute to an understanding of the molecular order of the adsorbed molecules was demonstrated.

The interface between implants and surrounding host tissues plays a crucial role in the success of implants [103]. The implant's surface morphology conditions the clinical success of titanium implants. Since titanium is still one of the most used and successful implanted biomaterials, it has been

investigated with AFM in several studies [87,104–109]. Often these characterisations of titanium or titanium alloy surfaces are carried out in combination with complementary surface analytical techniques such as X-ray photoelectron spectroscopy (XPS), secondary ion mass spectroscopy, Auger electron spectroscopy or contact angle measurements. Taborelli et al. [106] for example characterised the surfaces of four different titanium implants with AFM. The peak-to-valley and RMS roughness of the samples, either polished (P), polished and acid etched, sandblasted with large grit and acid etched, and sandblasted and submitted to titanium plasma spraying (TPS), varied strongly depending on the surface treatment. The P sample showed the smallest RMS roughness of 6 nm over a 20×20 μm^2 surface area, whereas the TPS sample was the roughest and this roughness exceeded the z-range of the AFM. No major differences in surface chemical composition where found by AES and all samples were hydrophobic. This study showed that the surface treatment of the implants had a significant effect on the surface morphology whereas the surface chemistry was only little affected by the treatments [106]. Fig. 9a and b show AFM images of two different titanium implant surfaces [109].

When interpreting the surface roughness values of biomaterials obtained with AFM, several points have to be considered. Surface roughness RMS or R_a values obtained from different biomaterials with AFM can only be compared if the area of which this value was obtained is stated and of similar size. Currently a large variation of surface area sizes exists in the literature reporting AFM roughness measurements of biomaterials. Because the biological components such as tissues, cells, plasma proteins, ligands etc. cover a wide range of length scales, a roughness measurement on appropriate logarithmic scales (i.e., 100 μm × 100 μm, 10 μm× 10 μm, ..., 1 nm × 1 nm) appears to be appropriate. Furthermore, details about the AFM tip used, especially the tip geometry, should be given, as roughness values of samples with steep trenches and groves obtained with pyramidal tips are likely to be false. It is hoped that in the future a correlation between physical parameters of biomaterials such as surface roughness and their biological performance can be established [110].

The surface roughness of the titanium implants discussed above hinders studying the adsorption of proteins on these surfaces with molecular resolution (see Sections 2.4 and 4) although progress has been made recently in imaging proteins on rough surfaces [109,111] by using AFM phase imaging. So far AFM imaging with true molecular resolution was limited to smooth 'model' surfaces such as HOPG, mica, or SAMs. Recently a titanium

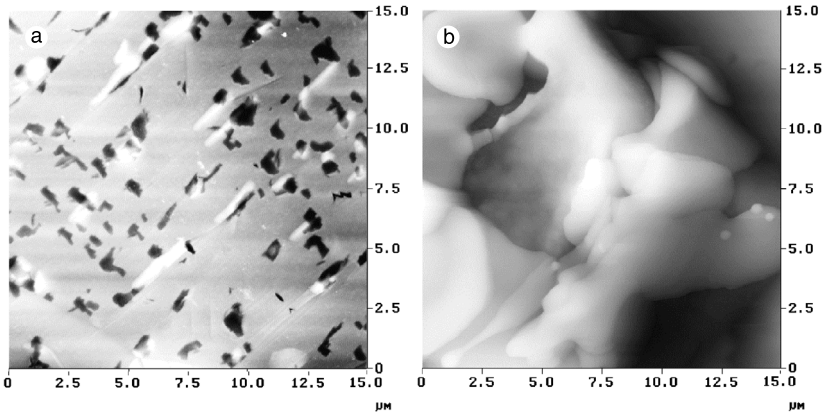

Fig. 9. (a) and (b): Mechanically polished titanium implant surface (a) (ground on silicon carbide paper, 1200 grit, and polished with colloidal silica). The polishing process leaves a mirror polished surface with pits. AFM tapping mode in air, z-range 50 nm. Plasma sprayed titanium (b) (sand blasted with alumina 250–500 μm and air plasma sprayed). The final plasma spraying process produces large curved structures on the titanium surface. AFM tapping mode in air, z-range 2.50 μm. Images after [109].

oxide substrate has been developed [87] which has a chemical composition similar to that of clinically used titanium implants and is ultra-flat. The latter makes it suitable for high-resolution studies of protein adsorption with AFM. The substrate is produced using a mica surface as template for the ultra flat titanium (titanium stripped template, TST, see Section 2.4). The TST samples show an RMS roughness of 0.29 ± 0.03 nm over 1.00×1.00 μm^2 areas (Fig. 10a). Atomic resolution of the titanium oxide surfaces was obtained with AFM as shown in Fig. 10b. Different degrees of molecular order were found on the titanium oxide surface. Incrystalline surface areas square lattices with para-meters $a_0 = b_0 \approx 0.5$ nm were resolved, which is consistent with the (0 0 1) planes of the titanium dioxide TiO_2 rutile. The chemical composition of this substrate increases the clinical relevance of AFM protein adsorption studies using this material.

4. Biomaterial interfaces with biomolecules

Biomaterials implanted in the human body adsorb proteins on their surfaces within a few seconds [103]. Subsequently cells arrive at the surface, interacting with the adsorbed protein layer. The bioreaction to a biomaterial is therefore affected by the initial event of protein adsorption, which then influences any further biological reaction. When adsorbing to a surface, protein molecules may undergo non-covalent structural transitions [112] and may change the exposition and orientation of their functional sites. Hence, the adsorbed protein layer may promote subsequent reactions that would not be caused by the same protein in its native conformation. Some biomaterial-tissue interactions, such as osteointegration or drug delivery, are beneficial to the host. Others however are aberrations of physiological processes and result in complications, such as inflammation, activation of the immune system, or thrombosis.

Although the knowledge of protein adsorption processes has increased rapidly over the last decades [113,114] the interaction of individual proteins with biomaterials, an important example being titanium oxide, remains poorly understood on a molecular level. Major reasons for this are the difficulties involved with imaging proteins on biomaterials surfaces with molecular resolution, especially under aqueous conditions.

Therefore, AFM has been applied to study protein-biomaterials interfaces. Examples for these studies include fibronectin [115,116] and human plasma fibrinogen (HPF) [86] on PMMA, HPF on

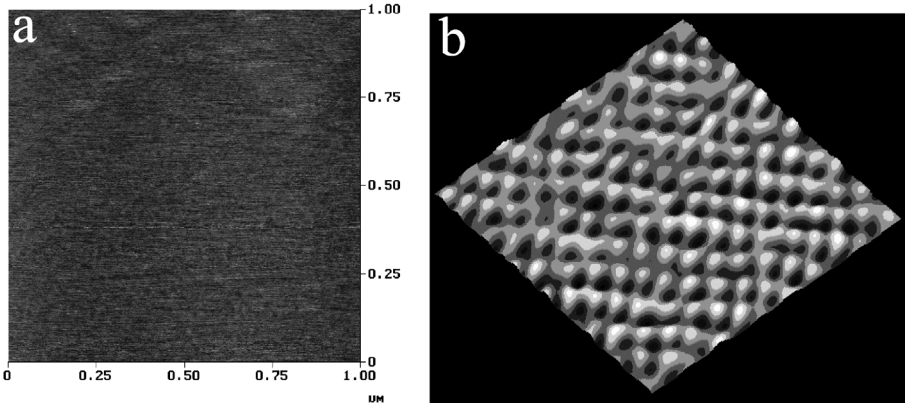

Fig. 10. (a) and (b): AFM images of ultra-flat TiO_2 sample surfaces produced by a template stripping method after [87]. At an image size of 1×1 μm^2 (z-range 1 nm) the sample surface appears almost featureless due to its flatness (a). High resolution imaging of the TiO_2 sample surfaces (b) shows atomic resolution of the (0 0 1) TiO_2 rutile with tetragonal lattice parameters of $a_0 = b_0 \approx 0.5$ nm (image size 5×5 nm^2, z-range 0.5 nm). TiO_2 is frequently used in implants and the samples presented here are suitable to obtain molecular resolution of absorbed biomolecules with AFM. Images after [87].

PTFE [117] or on SAMs [118,119], POE surfaces containing bovine serum albumin [120], fibronectin [107] and HPF [87] on titanium oxide, different plasma proteins on heparinised PVC [121], von Willebrand factor on SAMs [79] and template-imprinted nanostructured surfaces for protein recognition [122]. These and other AFM studies of protein–biomaterial interfaces have a great variety in surface physical (e.g. roughness, structure etc.) and chemical (composition) properties of the biomaterials, the selected proteins and experimental conditions. AFM studies of protein–biomaterial interfaces are carried out in air [116], in distilled water [87] or in buffer [118] at different temperatures. It is therefore difficult to directly compare results from different studies in many cases. Often these studies use complementary spectroscopic methods such as XPS (ESCA) [107,116] or contact angle measurements [116] to characterise the biomaterial surfaces' physico-chemical properties and the amount of adsorbed protein. The results from these experiments are then interpreted in conjunction with the results from the AFM experiments.

Typical aims of AFM studies of protein–biomaterial interfaces are to characterise the morphology of the adsorbed superstructures or the conformation and size of individual adsorbed protein molecules as a function of biomaterial composition and/or surface treatment. In addition, protein patterning and recognition [122,123], and the measurement of adhesion forces between protein molecules and biomaterial surfaces [124] have been explored with AFM. AFM images of adsorbed proteins presented in the majority of the protein–biomaterial interface studies are of relatively low resolution, i.e., they show protein networks or other superstructures of adsorbed proteins [120,121]. Fewer papers present persuasive molecular resolution of the adsorbed proteins [79, 86, 87,117–119,125] and a small number of studies show convincing details within individual protein molecules adsorbed on biomaterials, [79,87,118, 119].

In an early AFM investigation supported by XPS (ESCA), dynamic contact angle measurements of human plasma fibronectin (HFN) adsorbed on TiO_2 and PMMA revealed that the spreading of the adsorbed HFN depended on the chemical composition and the solid surface tension of the biomaterial surfaces [116]. The structure of the adsorbed HFN appeared as extended strands when imaged with contact mode in air AFM. The dimensions of HFN depended on the deposition method (spraying or droplet deposition). In addition, the dimensions of HFN appeared to be dependent on the tip shape and capillary forces.

The study of HPF conformations adsorbed on biomaterials is of very high relevance as this plasma protein plays a central role in the regulation of haemostasis, and surface induced thrombosis on biomaterials such as those used in cardiovascular devices [126]. A number of AFM studies focus on HPF adsorbed on different biomaterials, which is therefore discussed in more detail below.

The three-dimensional structure of HPF adsorbed on different SAMs [118,119] has been studied with tapping mode in fluid (buffer) AFM using ultra-sharp tips. These studies show molecular resolved HPF in the adsorbed state. Hydrated fibrinogen monomers were visualised as overlapping ellipsoids on octadecyltrichlorosilane (OTS). HPF dimers and trimers exhibited linear conformations predominantly and an increased affinity for the hydrophobic SAM surface compared to monomeric HPF [118]. HPF monomers show the typical trinodular structure with two D domains and an E domain and a molecular length of 48 ± 6 nm. The height of HPF monomers was measured to be 1.3 ± 0.3 nm. While the mean fibrinogen length was not found to be different from previous EM investigations, the mean minor axis dimensions showed marked deviation, which was attributed to imaging HPF in the hydrated state and to globular domain spreading after adsorption.

To study the surface dependency of the HPF conformation, these initial studies were later extended to three different, hydrophobic, positively charged OTS and 3-aminopropyltriethoxysilane (APTS) and negatively charged (mica) surfaces [119]. This study was carried out with the AFM operating in tapping mode in fluid using ultra-sharp tips. Quantitative dimensional analysis of the HPF structure adsorbed on the three substrates indicated that the surface-dependent structural

deformation or spreading of fibrinogen increases according to the order mica < APTS < OTS. Molecular length and D and E domain width of HPF increased while the corresponding heights decreased. The observed molecular lengths of HPF were 48.5 ± 4.3 nm on mica, 55.7 ± 6.4 nm on APTES and 63.7 ± 7.0 nm on OTS [119], the latter value being significantly larger than the value found in a previous study [118]. Obviously, the materials surface properties affect the conformational state and spreading of adsorbed HPF.

Recently, HPF adsorption on PMMA [86] and TiO_2 [87], both ultra-flat prepared, has been studied with high resolution AFM. The HPF adsorbed on PMMA was studied directly after protein adsorption and a rinsing step with tapping mode AFM in air. An AFM image of HPF molecules adsorbed on PMMA is shown in Fig. 11 [86]. The adsorbed HPF molecules show the distinct trinodular ('three beads on a string') structure with a molecular length of 48 ± 4 nm [86] and a height of 2.5 ± 0.4 nm [87]. Single molecules often exhibited a linear conformation and, in some cases, an L-shaped conformation where the two sub-units of the molecules were not aligned straight but formed an angle. The two spherical D domains and the central E domain of the HPF were revealed by the AFM. The observed HPF structure as well as the molecular length is comparable with those of HPF adsorbed on mica [119] and OTS [118] in previous studies. This is remarkable as PMMA has a more polar (hydrophilic) character than OTS through its polar carbonyl groups. In addition, the measurements were carried out in air shortly after rinsing steps, i.e., the HPF may still have been hydrated to a certain extent.

When investigating adsorbed HPF on TiO_2 [87], individual molecules and aggregates, often joined through their D domains, were resolved, and the typical HPF multiglobular structure was observed. The mean length and height of single molecules were 46 ± 3 nm and 1.4 ± 0.2 nm, respectively. Ultra-high resolution AFM imaging of individual HPF molecules showed additional features (chain segments) adjacent to the D and E domains. These were attributed to the α chains and their C-termini (Fig. 12). In addition to the high-resolution conformation of HPF, the same study showed atomic

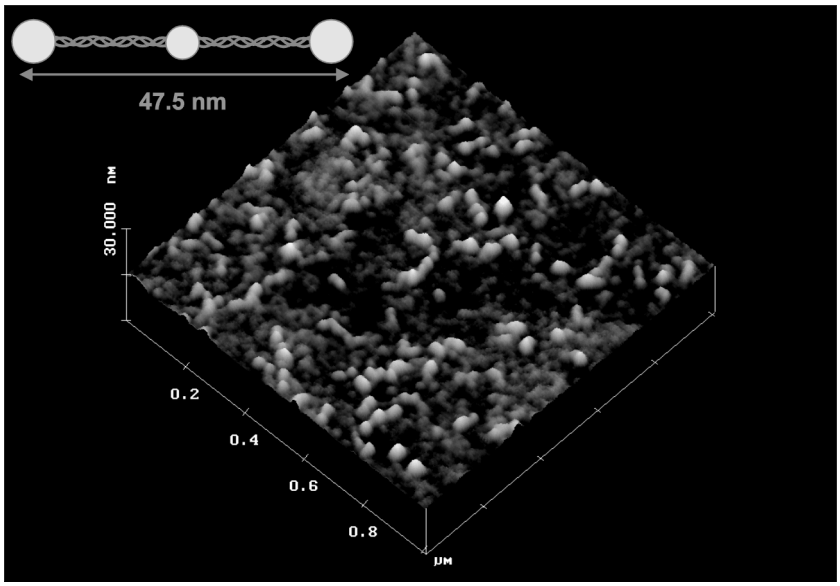

Fig. 11. AFM tapping mode in air image of human plasma fibrinogen (HPF) adsorbed on a spun cast ultra-flat PMMA surface (image size 1×1 µm^2, z-scale 30 nm). This image resolves individual HPF molecules as well as globular domains within the molecules. The length of the HPF molecules was measured to be 48 ± 4 nm [86] and the height 2.5 ± 0.4 nm. A model of the trinodular HPF molecule is inserted in the upper left corner of the image (drawn not to scale). Image after [86].

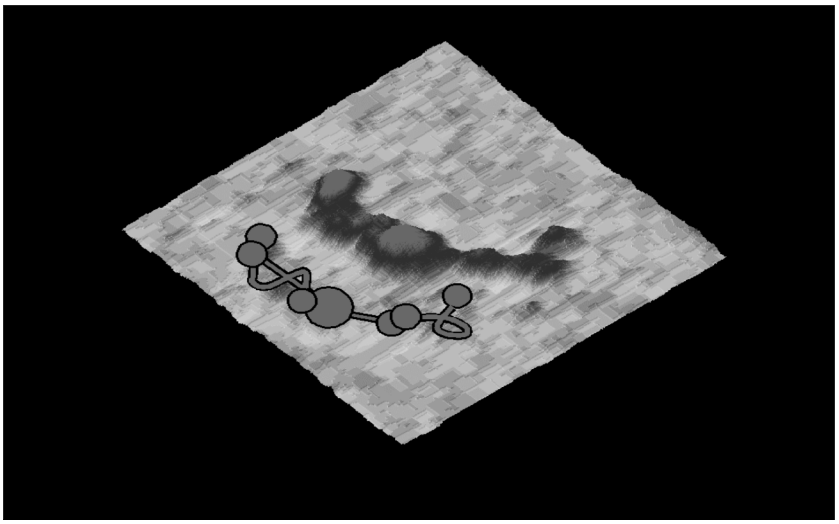

Fig. 12. High resolution image of a HPF macromolecule adsorbed on an ultra-flat TiO_2 sample similar to that shown in Fig. 10. The length of the HPF molecule is approximately 48 nm. Individual globular domains within the molecules as well as chain connector regions between the globular domains can be seen in this AFM tapping mode in fluid image. A model interpreting the AFM observation is shown as well in the image. Image after [87].

resolution of the underlying titanium oxide substrate. Further studies in this direction may show more detail about blood clotting pathways on biomaterials and the relative orientation of materials and biological molecules on a nanometer scale.

The ability of the AFM to explore conformational changes of matter on a molecular scale and to probe mechanical properties can be exploited in the investigation of biomaterial–biomolecule interfaces. von Willebrand Factor (vWF) plays a central role in the regulation of haemostasis and thrombosis by facilitating adhesion, aggregation and spreading of activated blood platelets [127]. This role is unique to the vWF under high shear conditions [128] such as present in microcirculation, stenosed arteries or cardiovascular devices. vWF was imaged with contact mode AFM with molecular resolution under different locally applied shear forces (7.4–19 nN) [79] after the application of shear stress of 0–42.2 dyn/cm^3. The substrates on which vWF were studied were OTS SAMs. A shear stress induced conformational transition from a globular state to an extended chain conformation at 35 dyn/cm^3 was observed. vWF molecules in their globular state have dimensions of 149×77 nm^2 and a height of 3.8 nm. The vWF molecules unfold to extended chains of molecular lengths ranging from 146 to 774 nm. vWF thrombogenetic properties appear to depend on shear stress induced structural changes of vWF in areas of high shear stress [79]. Latest research explores the intramolecular binding sites on surface-bound vWF under aqueous conditions with AFM [129].

Most of the biomaterials and model substrate systems discussed so far allow molecular resolution of adsorbed proteins because of their extreme flatness (see also Section 2.5). In these examples, the adsorbed protein can well be distinguished from the topographical background of the ultra-flat substrates. Clinically used biomaterials, however, are much rougher. Their roughness has prevented AFM observation of adsorbed proteins. Recently it was reported that individual HPF molecules were detected with phase imaging AFM on rough poly(dimethylsiloxane) (PDMS) and low-density poly(ethylene) (LDPE) biomaterials surfaces [111]. The samples exhibited RMS roughness 1.6 nm (PDMS) and 6 nm (LDPE), respectively over a 2.00×2.00 μm^2 area. The experiments were carried out in tapping mode in protein (buffer) solution. Although in AFM height images no proteins

adsorbed on these materials were observed, the simultaneous phase imaging showed evidence of adsorbed protein molecules and allowed the distinguishing of these molecules form the supporting biomaterial. As outlined in Section 2.2 and pointed out by the authors of this study [111] the imaging contrast is caused by different mechanical properties of biomaterials and the proteins, respectively. On expanded poly(tetrafluorethylene) (ePTFE), however, AFM phase imaging was not able to distinguish between the biomaterial and the HPF. Three potential explanations for this observation were given. No proteins adsorbed to the PTFE surface, or the surface RMS roughness of 23 nm was too large to give a phase contrast or, most likely, the adsorbed protein formed a closed film which gave a uniform phase contrast with no evidence (image phase contrast) from the supporting substrate. In this issue of 'Surface Science', Cacciafesta et al. report AFM phase imaging of adsorbed HPF protein films on TiO_2 implant surfaces with a RMS roughness of 8 and 160 nm over 20×20 μm^2 areas [109].

Proteins normally show a high affinity to many biomaterials surfaces and may induce specific body reactions after adsorption on biomaterials. One reaction is the activation of the complement system, which is part of the immune system [130] and includes classical activation pathways involving complement factors 1q (C1q) which binds the Fc part of slightly denatured immunoglobulin G (IgG). C1q bound on surfaces causes the formation of enzymatically active complexes, which cleave complement factor 3 (C3) into its active forms C3a and C3b [130]. The early events of classical complement activation have been studied with AFM in combination with immunological methods [131]. Serum protein adsorption on IgG-coated methyl terminated silicon surfaces followed by subsequent binding of anti-C1q and anti-C3c was observed with tapping mode in air AFM. Exposure to anti-C1q or anti-C3c after 15 s serum incubation showed a C1q submonolayer adsorbed. Increased incubation times of 1 min or more in serum followed by antibody incubations showed a decreased deposition of anti-C1q and increased anti-C3s binding supporting the hypothesis that activated C3b binds to and forms multilayers on the C1q containing complexes. The access of anti-C1q to its antigen is thereby prevented [131]. Further studies carried out on biomaterials may in the future give a better insight into complement activation reactions at biomaterial surfaces.

AFM force spectroscopy is a fascinating option to learn more about interactions at biomaterial–biomolecule interfaces. This method allows for example the study of the time dependence of the anchoring processes of biomolecules [132]. Force spectroscopy AFM has been used to investigate the kinetics of HPF adsorption on silica surfaces [132]. HPF molecules attached to an AFM tip were brought into contact with silica surfaces and approach/retraction cycles of the AFM tip were used to measure the HPF/silica interactions. Interaction times varied between 5 and 2000 ms. It was found that the minimal interaction time for an HPF molecule to bind strongly to the silica surface during an adsorption process lies between 50 and 200 ms. When the tip was retracted from the surface, multiple consecutive ruptures were observed. The number of ruptures increased steadily with interaction time as well as the mean rupture strength, which varied between 300 pN for 5 ms and 1400 pN for 2000 ms. This behaviour was explained by the assumption that a polymeric HPF chain interacts with the surface and the multiple interactions of this chain do not establish simultaneously but consecutively. The distance distribution between two consecutive ruptures showed a maximum around 20–20 nm, which corresponds to the distance between D and E domains of the HPF molecules. This indicated that HPF mainly adsorbed through its D and E globular domains to the substrate [132].

AFM has been used to quantitatively interrogate micropatterned biomolecules including quantification of recognition forces between proteins and their antibodies [123]. Precise quantification of biorecognition forces is necessary for comparison of different surface preparations. Micropatterned surfaces of osteopontin (OPN), a protein which plays an important role in bone remodelling, implant calcification and wound healing [133,134], have been prepared by microcontact printing (μCP) [123] on bovine serum albumin or mica, and imaged with AFM. The precise dimensions of the μCP such

as the OPN layer thickness of 2.5–3.5 nm were quantified with the AFM. For the quantification of the binding forces between OPN μCP surfaces and the antibody α-OPN, AFM tips were functionalized with the latter and force–piezoretraction curves were measured. From the measurements and an analysis of the frequency of the unbinding forces, an average antibody–antigen recognition binding force of 271 pN was calculated which is in good agreement with the value reported in the literature for antibody–antigen binding systems (49–244 pN) [123].

5. Surfaces and interfaces of mineralised tissues explored with AFM

One of the most active areas of the application of AFM in biomaterials science is mineralised tissue research. Within these research activities two main directions exist, the characterisation of mineralised tissue with AFM and the studies of demineralisation of mineralised tissue with AFM. Both areas are highly relevant in the area of oral biomaterials where restorative materials are bonded to the mineralised tissues, enamel and dentine. As a preparative step to enhance bonding between oral biomaterials and for example dentine, etching or conditioning agents are applied to the dentine [135]. Therefore, a need exists to understand the microscopic structure of mineralised tissues before and after the application of demineralising etching agents.

AFM studies of human and animal tooth enamel focus on the enamel fine structure [136–139], enamel demineralisation [136–144] enamel development [145,146] or nanomechanical properties of tooth enamel under a range of conditions [147, 148]. Tooth enamel studied with AFM showed hydroxyapatite (HA) crystals [136,137], distinct patterns of prismatic and aprismatic enamel [137, 139] and high resolution images of the (0 0 1) crystal faces of HA crystals with characteristic hexagonal shape and 60° angles between the (1 0 0) faces [137] were observed. An AFM image of prismatic and aprismatic human enamel of the buccal surface of a premolar is shown in Fig. 13.

Demineralisation studies of enamel have focused on the effects of different acids (such as phosphoric acid or citric acid) present in restorative dentistry etching agents or certain acidic foods, e.g., cola drinks or orange juice to enamel. Since the acidic constituents of the dental etching agents and some foods, especially acidic soft drinks, are quite similar and the experimental challenges of measuring demineralisation caused

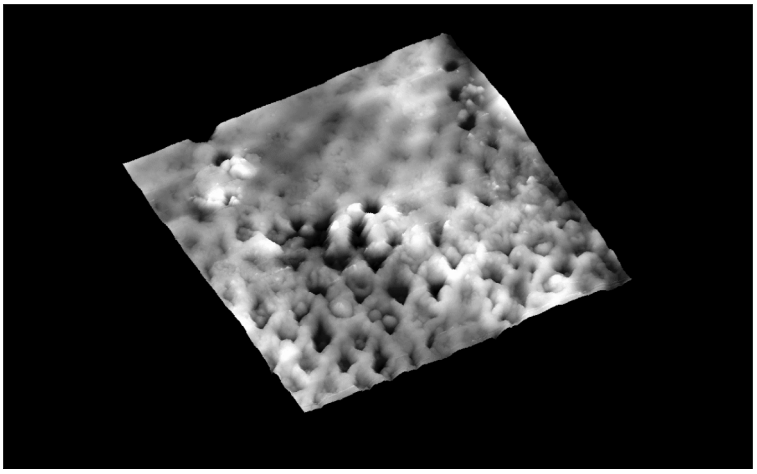

Fig. 13. Native human enamel surface imagined with tapping mode AFM. The sample was taken from a buccal surface (surface facing the cheeks) of a premolar. The image size is 75×75 μm^2 (z-range 2 μm). Prismatic (flat, rear of image) and aprismatic enamel (pitted, front of image) can be clearly distinguished in the image. Image after [139].

by both are strongly related, examples of demineralisation studies from both fields are included in this section.

In enamel demineralisation studies the AFM is used to explore the effects these acidic agents have on the structure of enamel and to precisely measure enamel material losses (AFM metrology) due to etching. Structural changes of polished enamel and enamel loss caused by acids in soft drinks using the AFM's fluid cell [140] have been studied. In this study, the enamel was exposed to the fluids in the AFM and images were recorded at different etching times as the dissolution of the polished enamel progressed. Successive images of the same areas were subtracted from each other and the maximal and minimal height changes in the differential images were measured. This study showed visible changes in surface morphology of the enamel as the dissolution progressed. Nevertheless absolute material losses or dissolution rates cannot be measured reliably with this method since all imaged enamel areas are affected by dissolution and no reference area which would not be affected by dissolution could be used. Potentially one can measure height differences between two successively taken AFM images by recording the voltage of the z-position of the AFM's piezoscanner as was attempted in this study [140]. Drift and instability [28] of the z-position and voltage, however, limit the usefulness of the results obtained in such a way.

The effect of fundamental acid agents of 2% phosphoric acid, 10% citric acid and 10% polyacrylic acid on the dissolution of polished enamel surfaces has been investigated in real time with AFM [143]. Consecutive scans of the enamel samples exposed to the acidic solutions were carried out. Contact mode AFM in fluid was used for this study. The changes of the surface topography of the etched enamel were recorded and differences in maximum etching depths and the etching rate were determined. Similar to the approach used in the study discussed previously only relative height changes can be measured with AFM by this method, since there is no stable height reference (area) against which the height changes can be measured. Rather than reporting etching depths, RMS values should be reported, as this would avoid confusion with absolute height measurements.

To solve the problem of reference areas for height measurements of mineralised tissues, different strategies have been developed. Enamel can be polished and subsequently partially covered with a protective tape before exposure to acids [139,141]. The protective tape is removed after the acid exposure and the resulting flat area can be used as a height reference in comparison to the dissolved enamel regions as shown in Fig. 14. With this method enamel dissolution based height differences on enamel can be measured with nm resolution [139,141]. The disadvantage of this method is that the enamel needs to be flattened (polished) and may differ in composition and structure from native enamel. In addition, this method is not suitable for measurements where the sample stays in the AFM, as the protective tape needs to be removed after the etching steps and before the AFM measurements.

As a more realistic alternative to polished enamel, native enamel was used in an enamel dissolution study [144] and a method previously developed to create a reference layer for AFM measurements on dentine [149] was adapted. For this end, a gold reference layer was evaporated onto part of a native enamel surface. This allowed precise measurements of the enamel dissolution caused by different acids present in soft drinks expressed as height difference between the reference layer and the acid exposed enamel surfaces by subtracting AFM images before and after the etching step. The error of this method, mainly caused by slight mismatches of the overlaid AFM images, was estimated to be 50 nm [144]. Based on measurements at different exposure times, time dependent dissolution equations have been proposed for the tested drinks. Titrable acidity, pH, mineral content and degree saturation of calcium hydroxyapatite of the soft drinks have been identified as factors influencing the enamel dissolution. Fig. 15 shows an example of a native enamel surface exposed to an acidic soft drink and a height profile of the native enamel/dissolved enamel interface (subtracted image).

Opposed to enamel, which forms the outer layer of teeth and has been explored with AFM in its

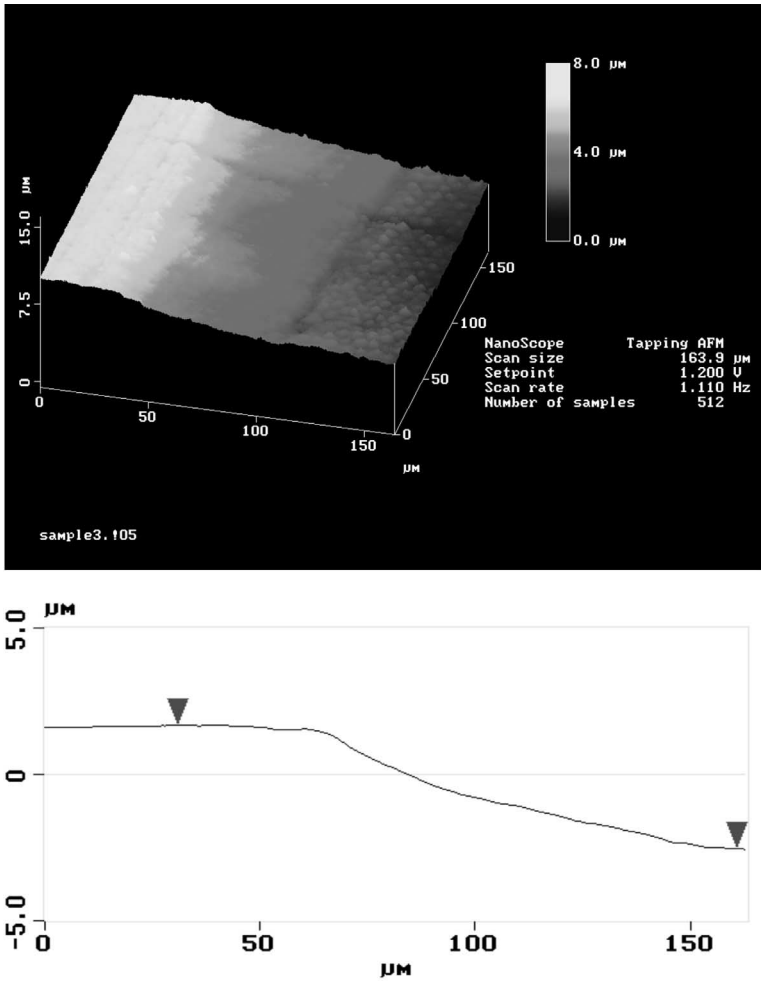

Fig. 14. AFM image (top) and corresponding topography section analysis (bottom) of a human polished enamel surface exposed to an acidic soft drink. The left area of the polished enamel surface was protected against dissolution by a protective tape during the exposure to the drink. After the exposure the tape was removed and the flat surface area was used as reference for height measurements of the enamel loss. An enamel loss of 4 μm was measured. The dissolution process has caused a material loss in the periphery of the enamel prisms (right sample area). Images after [139].

native and polished states, tooth dentine is normally only accessible after preparative steps such as cutting and polishing. Dental cavity preparation leaves a so-called smear layer on the dentine surface which has a thickness of several microns and consists of organic and inorganic debris produced during cavity preparation with a dental drilling instrument. To enable effective bonding of biomaterials to dentine this smear layer must be removed or modified to allow access to the underlying dentine [135]. For that end, acid solutions called conditioners are used on dentine.

Marshall and Balooch and co-workers [68,149–154] and other authors [85,155–162] have made a large number of significant contributions in the investigation of dentine with AFM. Aims of these studies were to explore acid etching or conditioning of dentine, [68,149,152–154,156,157,159–162], mechanical properties of native [150] and demineralised [151] dentine, collagen structure in

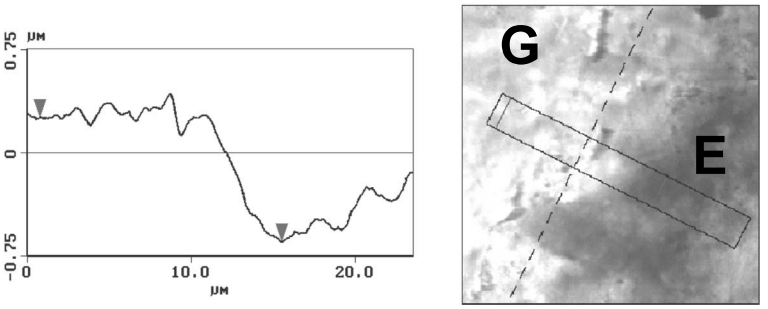

Fig. 15. AFM image (differential image, right) and corresponding topography section analysis (left) of a human native enamel surface exposed to an acidic soft drink. Successive images of the same surface area were subtracted from each other and the maximal and minimal height changes in the shown differential image were measured. Part of the surface was covered with a gold reference layer (G) and the height difference between this reference area and the dissolved enamel surface area (E) was measured to be 0.9 μm with a section analysis. A rectangular box in the AFM image indicates the analysed area. Image size 25 × 25 μm^2 (z-range 1.5 μm). The lines between which the height differences were measured are shown within the box. Images after [144].

dentine under different conditions [157,158,160], interfaces between adhesive biomaterials and dentine [85,155].

Contact mode in fluid AFM studies of the early stages of acid treatment of dentine revealed a preferential attack of 0.025 M nitric acid on peritubular dentine [68]. The intertubular dentine surface was dissolved initially at approximately half the rate of peritubular dentine and then reached a plateau as the demineralised collagen scaffold collapsed. The design of this study (acid exposure in the AFM's fluid cell) allowed following the etching process in real time. Differences in dentine morphology and etching rates are of importance for dentine bonding applications used with oral biomaterials relying on the penetration of the demineralised matrix by adhesive monomers. Since no stable reference area was used in this study, surface depth changes measured were only relative, i.e. maximal depths of the dentine surfaces were measured as a function of time.

Absolute depth changes of dentine exposed to either ethylenediamine tetracetic acid (EDTA), dilute phosphoric acid or citric acid in AFM contact mode in air experiments were measured in a later study [149]. These measurements were made possible due to the application of a gold reference layer to part of the dentine surface. This reference layer is assumed stable under the conditions of the experiment. The dentine surfaces treated with the different etching agents altered in different ways. The initial subsidence rates for the different agents were equal and linear. After an initial 100 nm depth change the intertubular dentine etching rates increased. The intertubular surface remained uniform and smooth for phosphoric acid and citric acid treatments. EDTA treatment left rough intertubular dentine surfaces. Consistent with a previous study [68] the surface subsidence reached a plateau after a depth change of about 0.5 μm, which resulted from a limit to the contraction of the demineralised and hydrated collagen scaffold.

To minimise the tip–dentine interactions tapping mode AFM was used in a study of wet dentine, which explored the effects of phosphoric acid, and three different commercial conditioning agents on the surface morphology and R_a roughness of dentine [159]. In all investigated cases, the dentine treatment with the conditioning agents removed the smear layer, and opened and exposed the dentinal tubules, which is a prerequisite for good resin penetration and biomaterial bonding (Fig. 16). Samples treated with phosphoric acid showed evidence of weakly bound debris at the dentine surface and smear plugs in some tubules. The study revealed differences in the tubule diameter, tubule depth and surface roughness between dentine treated with the different agents. This was attributed to the different composition of the

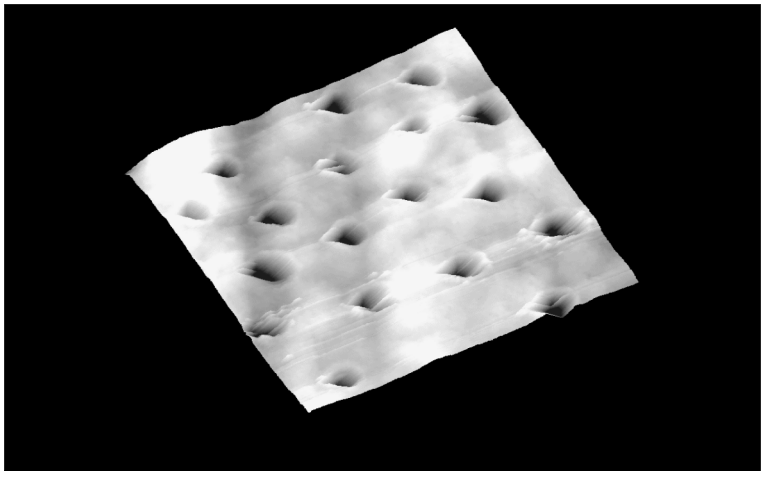

Fig. 16. AFM image of human dentine treated with Scotchbond 1 etching agent for 40 s. The dentine surface shows open dentinal tubules. Image size 170×170 μm^2 (z-range 8 μm). Image after [159].

agents and is useful in the selection of conditioning agents.

The effects of dentine depth, pH and different acids on dentine demineralisation were explored with contact mode AFM using a fluid cell [152]. This study allowed the quantification of changes during the etching of wet dentine with the help of a gold reference layer. Phosphoric acid and citric acid of different concentrations were used in this study. With a decreasing pH the peritubular etching rates increased. Changes were not linear with time and were different for the two acids studied over a similar pH range. The intertubular dentine surface recession was small and plateaued for low acid concentrations. The etching rate of peritubular and intertubular dentine did not depend on the depth of the dentine.

Dentine–biomaterial interfacial structures can be studied with AFM when cross-sectional AFM techniques are used. For this end, dentine–resin interfaces were sectioned with an ultra-microtome using a diamond knife [85] by adapting a method previously reported for the investigation of copolymer reinforced interfaces of homopolymers [36]. This resulted in smooth resin–dentine interfaces, which were imaged with tapping mode AFM in air. The samples prepared in this way show more detail at the interface than samples, which were flattened by mechanical polishing. Resin-tags in dentine, hybrid layer collagen, adhesive resin and unaffected dentine near the dentine–resin interface were observed with the AFM in this study. Cross-sectional microtoming techniques lead to smooth surfaces were the mechanical properties of the materials at the sectioned surface are similar [163,164]. In this case no height contrast is expected in tapping mode AFM [36]. In the discussed AFM study of dentine–resin interfaces [85], however, height differences of several hundred nm at the microtomed interfaces are presented. These height differences are likely to be the result of the different mechanical properties of the interfacial components. Collagen, resin and dentine may deform in a different way and the shear and compressive stresses applied by the microtome knife resulting in a non-flat surface finish. Great care must therefore be taken in the interpretation of the microstructure of sectioned mineralised tissue-biomaterial interfaces.

In the examples presented so far in this section AFM has been used as an imaging and metrology tool to measure and quantify minute changes in the surface topography of mineralised tissues. This section will conclude with two examples in which AFM is used to probe the mechanical properties of mineralised tissue. In a study by Kinney et al. AFM was used to measure the hardness and elasticity of fully hydrated peritubular and intertubular

human dentine [150]. For that end the standard AFM Si_3N_4 cantilever with typical stiffness of about 1 N/m was replaced with a stainless steel cantilever with a diamond tip and a stiffness of 646 N/m. During imaging of the dentine, forces of less than 10^{-6} N were applied whereas during plastic indentation the forces reached 268 μN. The indentation depths varied between 10 and 20 nm. The indentations were carried out in water to avoid dehydration of the dentine. From the measured projected area of the indentations and the applied force, it is possible to calculate (see Section 2.4 for details) the hardness for peritubular dentine of 2.3 GPa and for intertubular dentine of 0.5 GPa. The AFM force modulation mode enabled in the same study to image the stiffness properties of dentine. The peritubular dentine was measured to be stiffer than the intertubular matrix. As outlined in Section 2.2 FMM does not deliver absolute values of sample stiffness but shows surface areas of different stiffness as different image brightness. Furthermore, AFM nanoindentation, which does not use a vertical transducer tip but a cantilever, has a number of drawbacks (see Section 2.3).

Using an AFM with a vertical tip transducer specifically designed for nanoindentation, the mechanical properties of demineralised human dentine under three conditions, namely in water, in air after desiccation, and in water after rehydration, were measured [151]. The static elastic modulus (E_r^h 134 kPa) and the viscoelastic responses ($\tau_\varepsilon =$ 5.1 s and $\tau_\sigma = 6.6$ s) of the hydrated, demineralised collagen scaffolding were determined from the standard linear solid model of viscoelasticity. There were no significant variations of these properties observed with location. After a desiccation step, dentine showed considerably larger elastic moduli (2 GPa), and a hardness value of 0.2 GPa. Rehydration of the dentine samples led to a decreased elastic modulus but the value before dehydration (381 kPa) was not recovered.

6. Summary and outlook

AFM of biomaterials surfaces and interfaces has been discussed in this review paper with selected examples. The areas covered included theoretical and instrumental aspects such as AFM principles, working modes, types and accessories as well as limitations of AFM studies on biomaterials. AFM has been shown to be a helpful tool for the biomaterials scientist.

The use of AFM in biomaterials science and engineering is growing quickly. A number of different AFM techniques and accessories for the AFM are available today which enable the biomaterials scientist and engineer to study biomaterials with a minimum of sample preparation without destroying the sample. Interactions between single molecules and biomaterials surfaces can be explored with AFM single molecule spectroscopy, an important example being receptor–ligand interactions. AFM nanoindentation allows the measuring of hardness and reduced elastic modulus of biomaterials with small loads and high resolution. AFM is frequently used to characterise the surface topography and the properties of biomaterials. Material structure and properties are the focus of such studies. In vitro investigations of proteins at biomaterial surfaces under hydrated conditions open new opportunities to directly examine hypothesises of protein adsorption and as steps of the blood coagulation cascade, on a nanometer scale under near physiological conditions. Molecular and sub-molecular resolution AFM of protein–biomaterial interfaces deliver unsurpassed structural information and will potentially improve the future understanding of these interfaces. AFM investigations under 'close to physiological conditions' (in fluids at 37°C), may also help to elucidate pathobiological responses to implants such as inflammation, complement activation at biomaterials surfaces, restenoisis after vascular stenting, thrombosis of small-diameter vascular grafts or ectopic mineralisation of implants such as heat valves. In the area of mineralised tissues AFM is used as a versatile metrology tool to measure minute height changes of the tissues caused by acid attack and to study the morphology of mineralised tissues with or without contact to biomaterials.

To obtain useful information from biomaterials with AFM, careful sample preparation, which immobilises the biomaterial system, is required. The image quality in AFM is crucially influenced

by the tip quality (sharpness). Tip–sample interactions are essential for the imaging process and must be considered and monitored during the measurement, also to rule out artefacts. Combining AFM results from biomaterials with other experimental methods such as spectroscopic methods can strongly increase the understanding of the organic material system.

Future progress in the field of biomaterials explored with AFM depends strongly on new instrumental developments and on new ways of sample preparation. The introduction of the AFM tapping mode in fluid, i.e. the use of tapping mode in combination with a fluid cell for the analysis of biomaterials in a liquid medium is a major advance which reduces the amount of unwanted tip–sample interactions. Interesting developments such as AFMs with improved *Q*-factors and control [165] or the combination of AFM and NMR [166] will help to broaden the application of AFM in biomaterials science in the future. After the AFM has been shown to be capable of true atomic (and molecular) resolution and biological recognition, a prerequisite for understanding the bioreaction to implants and designing active and smart biomaterials is fulfilled.

Acknowledgements

KDJ gratefully acknowledges the help of Karin Jandt, Sally Gregg, Paola Cacciafesta and Manuela Finke in the preparation of this manuscript. KDJ thanks Paola Cacciafesta for preparing Figs. 1–4.

References

[1] G. Binnig, C. Quate, G. Gerber, Phys. Rev. Lett. 56 (1986) 930.
[2] K.D. Jandt, Mat. Sci. Eng. R21 (1998).
[3] S. Kaas, N.H. Thomson, B.L. Smith, P.K. Hansma, J. Miklossy, H.G. Hansma, Int. J. Imag. Sys. Techn. 8 (1997) 151.
[4] R.J. Colton, D.R. Baselt, Y.F. Dufrene, J.B.D. Green, G.U. Lee, Curr. Opin. Chem. Biol. 1 (1997) 370.
[5] H. Gaub, A. Engel, J. Struct. Biol. 119 (1997) 83.
[6] B. Drake, C.B. Prater, A.L. Weisenhorn, S.A.C. Gould, T.R. Albrecht, C.F. Quate, D.S. Cannell, H.G. Hansma, P.K. Hansma, Science 243 (1989) 1586.
[7] A.L. Weisenhorn, M. Egger, F. Ohnesorge, S.A.C. Gould, S.P. Heyn, H.G. Hansma, R.L. Sinsheimer, H.E. Gaub, P.K. Hansma, Langmuir 7 (1991) 8.
[8] H.K. Wickramasinghe, AIP Conf. Proc. 241 (1992) 9.
[9] S. Orisaka, T. Minobe, T. Uchihashi, Y. Sugawara, S. Morita, Appl. Surf. Sci. 140 (1999) 243.
[10] K.D. Jandt, T.J. McMaster, M.J. Miles, J. Petermann, Macromolecules 26 (1993) 6552.
[11] B. Baretzky, B. Reinsch, U. Taffner, G. Schneider, M. Ruhle, Z. Metallkunde 87 (1996) 332.
[12] D.V. Klinov, I.V. Lagutina, V.V. Prokorov, T. Neretina, P.P. Khil, Y.B. Lebedev, D.I. Chereny, V.V. Demin, E.D. Sverdlov, Nucleic Acids Res. 26 (1998) 4603.
[13] J.A. DeRose, J.P. Revel, Thin Solid Films 331 (1998) 194.
[14] F. Ohnesorge, G. Binnig, Science 260 (1993) 1451.
[15] A.F. Oberhauser, P.E. Marszalek, M. CarrionVazquez, J.M. Fernandez, Nature Struct. Biol. 6 (1999) 1025.
[16] C.M. Mate, G.M. McClelland, R. Erlandson, S. Chiang, Phys. Rev. Lett. 59 (1987) 1942.
[17] C.D. Frisbie, L.F. Rozsnyai, A. Noy, M.S. Wrighton, C.M. Lieber, Science 265 (1994) 2071.
[18] P. Maiwald, H.J. Butt, S.A.C. Gould, C.B. Prater, B. Drake, J.A. Gurley, V.B. Eilings, P.K. Hansma, Nanotechnology 2 (1991) 103.
[19] P. Grutter, D. Rugar, H.J. Mamin, Ultramicroscopy 47 (1992) 393.
[20] W.K. Zhang, Q.B. Xu, S. Zou, H.B. Li, W.Q. Xu, X. Zhang, Z.Z. Shai, M. Kudera, H.E. Gaub, Langmuir 16 (2000) 4305.
[21] H.B. Li, W.K. Zhang, W.Q. Xu, X. Zhang, Macromolecules 33 (2000) 465.
[22] M. Rief, H. Clausen-Schaumann, Nature Struc. Biol. 6 (1999) 346.
[23] E.L. Florin, V.T. Moy, H.E. Gaub, Science 264 (1994) 415.
[24] L. Liu, C.S. Jayanthi, M.J. Tang, S.Y. Tobler, C.W. Zhou, L. Alexseyev, J. Kong, H.J. Dai, Phys. Rev. Lett. 84 (2000) 4950.
[25] R. Resch, D. Lewis, S. Metzler, N. Montoya, B.E. Koel, A. Madhukar, A.A.G. Requicha, P. Will, Ultramicroscopy 82 (2000) 135.
[26] Sixth World Biomaterials Congress, 15–20 May Kamuela, Hawaii, USA, Transactions Vols. I, II, III, Society for Biomaterials USA, Minneapolis, 2000.
[27] D. Williams, Concise Encyclopedia of Medical and Dental Materials, Pergamon Press, Oxford, 1990.
[28] R. Wiesendanger, Scanning Probe Microscopy and Spectroscopy: Methods and Applications, Cambridge University Press, Cambridge, 1995.
[29] D.A. Bonnell, Scanning Probe Microscopy and Spectroscopy: Theory, Techniques, and Applications, Wiley, New York, 2000.
[30] C.F. Quate, Surf. Sci. 300 (1994) 980.
[31] H. Heinzelmann, E. Meyer, H. Rudin, H.-J. Güntherrodt, in: R.J. Behm, N. Garcia, H. Rohrer (Eds.),

Scanning Tunneling Microscopy and Related Methods, Nato ASI Series Vol. 184, Kluwer Academic, Dordrecht, 1990, p. 449.
[32] G. Binnig, H. Rohrer, IBM J. Res. Dev. 30 (1986) 355.
[33] T.R. Albrecht, S. Akamine, T.E. Carver, C.F. Quate, J. Vac. Sci. Technol. A 8 (1990) 3386.
[34] G. Binnig, D.P.E. Smith, Rev. Sci. Instrum. 57 (1986) 1688.
[35] C.J. Chen, Introduction to Scanning Tunneling Microscopy, Oxford University Press, New York, 1993.
[36] K.D. Jandt, C.-A. Dai, E.J. Kramer, Adv. Mat. 8 (1996) 660.
[37] Q. Zhong, D. Innis, K. Kjoller, V.B. Elings, Surf. Sci. Lett. 290 (1993) L688.
[38] Phase Imaging-Beyond Topography, DI – Application Note, Digital Instruments, CA, USA, 1995.
[39] D. Raghavan, X. Gu, T. Nguyen, M. VanLandingham, A. Karim, Macromolecules 33 (2000) 2573.
[40] Y. Martin, C.C. Willimas, H.K. Wickramasinghe, J. Appl. Phys. 61 (1987) 4723.
[41] C. Girard, D. van Labeke, J.M. Vigoureux, Phys. Rev. B 40 (1989) 12133.
[42] D. Sarid, E. Elings, J. Vac. Sci. Technol. B 9 (1991) 431.
[43] E. Meyer, Prog. Surf. Sci. 41 (1992) 3.
[44] A. Kikukawa, S. Hosaka, Y. Honda, R. Imura, Rev. Sci. Instrum. 66 (1995) 101.
[45] F.M. Ohnesorge, Surf. Intern. Anal. 27 (1999) 379.
[46] H. Hosoi, K. Sueka, K. Hayakawa, K. Mukasa, Appl. Surf. Sci. 157 (2000) 218.
[47] MultiMode Scanning Probe Microscope Instruction Manual. Digital Instruments, Santa Barbara, CA, USA, 1996.
[48] T.J. Senden, W.A. Ducker, Langmuir 10 (1994) 1003.
[49] J. Cleveland, S. Manne, D. Bocek, P.A. Hansma, Rev. Sci. Instr. 64 (1993) 403.
[50] J.E. Sader, I. Larson, P. Mulvaney, L.R. White, Rev. Sci. Instr. 66 (1995) 3789.
[51] J.L. Hutter, J. Bechhoefer, Rev. Sci. Instr. 64 (1993) 1868.
[52] D.R. Baselt, J.D. Baldeschwieler, J. Appl. Phys. 76 (1994) 33.
[53] M. Radmacher, M. Fritz, J.P. Cleveland, D.A. Walters, P.K. Hansma, Langmuir 10 (1994) 3809.
[54] A.N. Parbhu, W.G. Bryson, R. Lal, Biochem. 38 (1999) 11755.
[55] T. Boland, B.D. Ratner, Proc. Nat. Acad. Sci. USA 92 (1995) 5297.
[56] Y. Harada, M. Kuroda, A. Ishida, Langmuir 16 (2000) 708.
[57] A.V. Kulkarni, B. Bhushan, Thin Solid Films 291 (1996) 206.
[58] K.D. Costa, F.C.P. Yin, J. Biomech. Eng. 212 (1999) 462.
[59] B. Bushan, Handbook of Micro/Nanotribology, CRC Press, Boca Raton, 1998.
[60] B. Bhushan, V.N. Koinkar, Appl. Phys. Lett. 64 (1994) 1653.
[61] B. Bhushan, A.V. Kulkarni, W. Bonin, J.T. Wyrobek, Phil. Magn. A 74 (1996) 1117.
[62] Digital Instruments, Nanoindentation and Hardness Testing with Nanoscope SPMs, Santa Barbara, CA, USA, 1997.
[63] Hysitron Inc., Minneapolis, MN, 55439, USA.
[64] N.A. Burnham, R.J. Colton, J. Vac. Sci. Technol. A 7 (1989) 2906.
[65] S.M. Hues, C.F. Draper, K.P. Lee, R.J. Colton, Rev. Sci. Instr. 65 (1994).
[66] S.M. Hues, C.F. Draper, R.J. Colton, J. Vac. Sci. Technol. B 12 (1994) 2211.
[67] W.C. Oliver, G.M. Pharr, J. Mat. Res. 7 (1992) 1564.
[68] G.W. Marshall, M. Balooch, R.J. Tench, J.H. Kinney, S.J. Marshall, Dent. Mater. 9 (1993) 265.
[69] M. Fritz, M. Radmacher, J.P. Cleveland, M.W. Allerma, R.J. Stewart, R. Gieselmann, P. Janmey, C.F. Schmidt, P.K. Hansma, Langmuir 11 (1995) 3529.
[70] M. Fritz, M. Radmacher, M.W. Allersma, J.P. Cleveland, J.S. Russel, P.K. Hansma, C.F. Schmidt, SPIE 2384 (1995) 150.
[71] J.L. OrtegaVinuesa, P. Tengvall, I. Lundström, J. Coll. Int. Sci. 207 (1998) 228.
[72] T.C. Ta, M.T. Sykes, M.T. McDermott, Langmuir 14 (1998) 2435.
[73] Y. Lyubchenko, L. Shlyakhtenko, R. Harrington, P. Oden, S. Lindsay, Proc. Nat. Acad. Sci. USA 90 (1993) 2137.
[74] A.P. Quist, L.P. Bjorck, C.T. Reimann, S.O. Oscarson, B.U.R. Sundquist, Surf. Sci. 325 (1995) L406.
[75] J.N. Israelachvili, Intermolecular and Surface Forces, Academic Press, New York, 1991, Chapters 16–18.
[76] A. Uhlman, Thin Films: Self-Assembled Monolayers of Thiols, vol. 24, Academic Press, New York, 1998.
[77] L.C. Giancarlo, G.W. Flynn, Rev. Phys. Chem. 49 (1998) 297.
[78] M.J. Hostetler, R.W. Murray, Current Opin. Coll. Interf. Sci. 2 (1997) 42.
[79] C.A. Siedlecki, B. Lestini, K. Kottke Marchant, S.J. Eppell, D.L. Wilson, R.E. Marchant, Blood 88 (1996) 2939.
[80] P. Wagner, P. Kernen, M. Hegner, E. Ungewickell, G. Semenza, FEBS Lett. 356 (1994) 267.
[81] D.M. Disley, D.C. Cullen, H.X. You, C.R. Lowe, Biosens. Bioelectron. 13 (1998) 1213.
[82] A.F. von Recum, C.E. Brown, C.E. Shannon, M. LaBerge, in: A.F. von Recum (Ed.), Handbook of Biomaterials Evaluation, second ed., Taylor and Francis, Philadelphia, 1999 (Chapter 13).
[83] Y.Z. Yang, J.M. Tian, J.T. Tian, Z.Q. Chen, X.J. Deng, D.H. Zhang, J. Biomed. Mat. Res. 52 (2000) 333.
[84] K.D. Jandt, Probe Micros. 1 (1999) 323.
[85] Y. Yoshida, B. Van Meerbeek, J. Snauwaert, L. Hellemans, P. Lambrechts, G. Vanherle, K. Wakasa, D.H. Pashley, J. Biomed. Mat. Res. 47 (1999) 85.
[86] K.D. Jandt, M. Finke, P. Cacciafesta, Coll. Interf. B 19 (2000) 301.
[87] P. Cacciafesta, A.D.L. Humphris, K.D. Jandt, M.J. Miles, Langmuir 16 (2000) 8167.

[88] M. Hegner, P. Wagner, G. Semenza, Surf. Sci. 291 (1993) 39.
[89] P. Wagner, M. Hegner, H.J. Güntherodt, G. Semenza, Langmuir 10 (1995) 3867.
[90] R.A. Latour, in: A.F. von Recum (Ed.), Handbook of Biomaterials Evaluation, second ed., Taylor and Francis, Philadelphia, 1999 (Chapter 3).
[91] J.J. Mecholsky, Dent. Mater. 11 (1995) 113.
[92] F.E. Martin, J. Dent. Res. 75 (1996) 2197.
[93] M.J.A. Braem, S. Gladys, P. Lambrechts, G.J. Vanherle, Dent. Res. 76 (SISI) (1997) 493.
[94] H. Ishida, in: H. Ishida (Ed.), Molecular Characterisation of Composite Interfaces, Plenum Press, New York, 1985, p. 25.
[95] K.J.M. Söderblohm, S.W. Shang, J. Dent. Res. 72 (1993) 1050.
[96] O.K. Johannson, F.O. Stark, G.E. Vogel, R.M. Fleischmann, J. Comp. Mat. 1 (1967) 278.
[97] K.D. Jandt, M. Bunk, M.J. Miles, J. Petermann, Polymer 35 (1994) 2458.
[98] S. Corneillie, P.N. Lan, E. Schacht, M. Davies, A. Shard, R. Green, S. Denyer, M. Wassail, H. Whitfield, S. Choong, Polym. Int. 46 (1998) 251.
[99] X. Chen, S.L. McGurk, C.J. Roberts, K.M. Shakesheff, S.J.B. Tendler, P.M. Williams, J. Davies, A.C. Dawkes, A. Domb, Macromolecules 31 (1998) 2278.
[100] N.B. Holland, Y. Qiu, M. Ruegesegger, R.M. Marchant, Nature 392 (1998) 799.
[101] T. Kanno, H. Tanaka, N. Miyoshi, T. Kawai, Jpn. J. Appl. Phys. Lett. 39 (2000) L269.
[102] M.C. Porte-Durrieu, C. Aymes-Chodur, N. Betz, C. Baquey, J. Biomed. Mat. Res. 52 (2000) 119.
[103] T.A. Horbett, B.D. Ratner, J.M. Schakenraad, F.J. Schoen, in: B.D. Ratner, A.S. Hoffmann, F.J. Schoen, J.E. Lemons (Eds.), Biomaterials Science: An Introduction to Materials in Medicine, Academic Press, San Diego, CA, 1996 (Chapter 3).
[104] M. Browne, P.J. Gregson, R.H. West, J. Mat. Sci. Mater. Med. 7 (1996) 323.
[105] D.V. Kilpadi, J.J. Weimer, J.E. Lemons, Coll. Surf. A 135 (1998) 89.
[106] M. Taborelli, M. Jobin, P. Francois, P. Vaudaux, M. Tonetti, S. Szumkler-Moncler, J.P. Simpson, P. Descouts, Clin. Oral Impl. Res. 8 (1997) 208.
[107] D.E. MacDonald, B. Markovic, M. Allien, P. Somasundaran, A.L. Boskey, J. Biomed. Mat. Res. 41 (1998) 120.
[108] H.E. Placko, S. Mishra, J.J. Weimer, L.C. Lucas, Int. J. Oral Maxill. Impl. 15 (2000) 355.
[109] P. Cacciafesta, K.R. Hallam, A.C. Watkinson, G.C. Allen, M.J. Miles, K.D. Jandt, Surf. Sci. 491 (2001) 405.
[110] B.D. Ratner in: B.D. Ratner, A.S. Hoffmann, F.J. Schoen, J.E. Lemons (Eds.), Biomaterials Science. An Introduction to Materials in Medicine, Academic Press, San Diego, CA, 1996, p. 445.
[111] N.B. Holland, R.E. Marchant, J. Biomed. Mat. Res. 51 (2000) 307.
[112] V. Hlady, J. Buijs, in: M. Malmstem (Ed.), Biopolymers at Interfaces, Dekker, New York, 1998, p. 181.
[113] T.A, Horbert, in: S.L. Cooper, N.A. Peppas (Eds.), Biomaterials: Interfacial Phenomena and Applications, ACS Advances in Chemistry Series, vol. 199, American Chemical Society, Washington, DC, 1982, p. 233.
[114] T.A. Horbett, Cardiovasc. Path. 2 (1993) 137S.
[115] R. Emch, F. Zenhausern, M. Jobin, M. Taborelli, P. Descouts, Ultramicroscopy 42–44 (1992) 1155.
[116] F. Zenhausern, M. Adrian, P. Descouts, J. Electron. Microsc. 42 (1993) 378.
[117] J.R. Rasmusson, R. Erlandsson, W.R. Salaneck, M. Schott, D.T. Clark, I. Lundström, Scann. Microsc. 8 (1994) 481.
[118] R.E. Marchant, M.D. Barb, J.R. Shainoff, S.J. Eppell, D.L. Wilson, C.A. Siedlecki, Thromb. Haemost. 77 (1997) 1048.
[119] P.S. Sit, R.E. Marchant, Thromb. Haemost. 82 (1999) 1053.
[120] K.M. Shakesheff, M.C. Davis, J. Heller, C.J. Roberts, S.J.B. Tendler, P.M. Williams, Langmuir 11 (1995) 2447.
[121] J. Yu, M. Nordman Montelius, M. Paulsson, I. Gouda, O. Larm, L. Montelius, Å. Ljungh, Biomaterials 15 (1994) 805.
[122] H. Shi, W.-B. Tsai, M.D. Garrison, S. Ferrari, B.D. Ratner, Nature 398 (1999) 593.
[123] M.D. Garrison, T.C. McDevitt, R. Luginbühl, C.M. Giachelli, P. Stayton, B.D. Ratner, Ultramicroscopy 82 (2000) 193.
[124] R. Eckert, S. Jeney, J.K.H. Hörber, Cell Biol. Int. 21 (1997) 707.
[125] R. Wigren, H. Elwing, R. Erlandsson, S. Welin, I. Lundström, FEBS Lett. 280 (1991) 225.
[126] S.R. Hanson, Cardiovasc. Pathol. 2 (1993) 157S.
[127] D. Meyer, J.-P. Girma, Thromb. Haemost. 70 (1993) 99.
[128] H.J. Weiss, J. Hawinger, Z.M. Ruggeri, V.T. Turitto, P. Thiagarajan, T. Hoffmann, J. Clin. Invest. 83 (1989) 288.
[129] M. Raghavachari, K. Kottke-Marchant, R.E. Marchant, Thromb. Res. 98 (2000) 351.
[130] P.J. Lachmann, N.C. Hughes-Jones, in: H.J. Müller-Eberhard, P.A. Miescher (Eds.), Complement, Springer, Berlin, 1985, p. 147.
[131] B. Wälivaara, A. Askendal, I. Lundström, P. Tengvall, J. Colloid Interf. Sci. 187 (1997) 121.
[132] J. Hemmerle, S.M. Altman, M. Maaloum, J.K.H. Hörber, L. Heinrich, J.-C. Voegel, P. Schaaf, Proc. Natl. Acad. Sci. USA 96 (1999) 6705.
[133] D.T. Denhardt, M. Noda, J. Cell Biochem. (30–31) (Suppl.) (1998) 92–102.
[134] M.D. McKnee, A. Naci, Conn. Tissue Res. 35 (1996) 197.
[135] J.D. Eick, A.J. Guinnett, D.H. Pashley, S.J. Robinson, Crit. Rev. Oral. Biol. Med 8 (1997) 306.
[136] S. Kasas, A. Berdal, M.R. Celio, SPIE Vol. 1855 Scanning Probe Microscopies II, 1993, p. 17.
[137] P. Schaad, E. Paris, F.J.G. Cuisinier, J.-C. Voegel, Scan. Micros. 7 (1993) 1149.

[138] M. Farina, A. Schemmel, G. Weissmüller, J. Struct. Biol. 125 (1999) 39.
[139] N.X. West, K.D. Jandt in: M. Addy, G. Embery, W.M. Edgar, R. Orchardson (Eds.), Tooth Wear and Sensitivity, Martin Dunitz, London, 2000, p. 105.
[140] O. Sollböhmer, K.-P. May, M. Anders, Thin Solid Films 264 (1995) 176.
[141] D.M. Parker, M. Finke, M. Addy, J. Hughes, E. Macdonald, K.D Jandt, J. Dent. Res. SI B 77 (1998) 1708.
[142] M. Finke, K.D. Jandt, D.M. Parker, J. Dent. Res. SI 79 (2000) 3687.
[143] F. Watari, J. Electron. Micros. 48 (1999) 537.
[144] M. Finke, D.M. Parker, K.D. Jandt, J. Colloid Interf. Sci. 232 (2000) 156.
[145] J. Kirkham, S.J. Brookes, R.C. Shore, D.A.M. Smith, M. Wallwork, C. Robinson, J. Dent. Res. 76 (1997) 1029.
[146] J. Kirkham, S.J. Brooks, R.C. Shore, W.A. Bonass, D.A. Smith, M.L. Wallwork, C. Robinsion, Connect. Tissue Res. 39 (1998) 91.
[147] H. Fong, M. Sarikaya, S.N. White, M.L. Snead, Mat. Sci. Eng. C 7 (2000) 119.
[148] M. Finke, J.A. Hughes, D.M. Parker, K.D. Jandt, Surf. Sci. 491 (2001) 456.
[149] G.W. Marshall, M. Balooch, J.H. Kinney, S.J. Marshall, J. Biomed. Mat. Res. 29 (1995) 1381.
[150] J.H. Kinney, M. Balooch, S.J. Marshall, G.W. Marshall, T.P. Weihs, J. Biomech. Eng. Trans. ASME 118 (1996) 133.
[151] M. Balooch, I.C. Wu-Magidi, A. Balazs, A.S. Lundkvist, S.J. Marshall, G.W. Marshall, W.J. Siekhaus, J.H. Kinney, J. Biomed. Mat. Res. 40 (1998) 539.
[152] G.W. Marshall, N. Inai, I.C. Wu-Magidi, M. Balooch, J.H. Kinney, J. Tagami, S.J. Marshall, Dent. Mater. 13 (1997) 338.
[153] J.I. Rosales, G.W. Marshall, S.J. Marshall, L.G. Watanbe, M. Toledano, M.A. Cabrerizo, R. Osoris, J. Dent. Res. 78 (1999) 1554.
[154] G.W. Marshall, K. Saeki, S.A. Gansky, S.J. Marshall, Am. J. Dent. 12 (1999) 271.
[155] C. Cassinelli, M. Morra, J. Biomed. Mater. 28 (1994) 1427.
[156] C. Cassinelli, M. Morra, J. Mat. Sci. Mater. M 5 (1994) 606.
[157] G. Eliades, G. Palaghias, G. Vougioklakis, Dent. Mater. 13 (1997) 24.
[158] F. El Feninat, T.H. Ellis, E. Sacher, I. Stangel, J. Biomed. Mat. Res. 42 (1998) 549.
[159] N. Silikas, D.C. Watts, K.E.R. England, K.D. Jandt, J. Dent. 27 (1999) 137.
[160] G. Eliades, G. Vougiouklakis, G. Palaghias, Dent. Mater. 15 (1999) 310.
[161] J. Perdigao, J.Y. Thomson, M. Toledano, R. Osoris, Am. J. Dent. 12 (1999) 250.
[162] S. Phrukkanan, M.F. Burrow, P.G. Hartley, M.J. Tyas, Dent. Mater. 16 (2000) 255.
[163] G.F. Mokotoff, Electron Microscopy Laboratory Techniques, Library Research Associates, Monroe, New York, 1990.
[164] L.C. Sawyers, D.T. Grubb, Polymer Microscopy, Chapman and Hall, London, 1996.
[165] A.D.L. Humphris, J. Tamajo, M.J. Miles, Langmuir 16 (2000) 7891.
[166] D. Rugar, O. Züger, S. Hoen, C.S. Yannoni, H.-M. Vieth, R.D. Kendrick, Science 264 (1994) 1560.